Establishing a blood plasma model for Sn(IV) with the two blood plasma ligands, Cysteine and Histidine.

BY

Ratanang Margin Senwedi

A dissertation submitted in partial fulfillment of the requirements for the degree of

Master of Science (Applied Radiation Science and Technology)

Supervisor: Dr Jan Rijn Zeevaart

Co-supervisors: Mr David R. Jansen
Ms Judith Wagener

Faculty of Agriculture, Science and Technology
(Center of Applied Radiation Science and Technology)

North-West University (Mafikeng Campus)

April 2008

DECLARATION

I declare that this dissertation is my own work, and has not been submitted to any University for the purpose of obtaining any degree. It is submitted for the fulfilment of the degree of Master of Science in the Faculty of Agriculture, Science and Technology of the North West University. Other sources of information have been noted by means of references.

Signature.....

Date.....25 November 2008.....

ABSTRACT

Bone pain secondary to metastatic bone cancer is the most common intractable pain and is a cause for major concern in most oncology units the world over. Bone metastasis occurs when cancerous cells from the primary tumor relocate to the bone.

There have been several traditional methods of treating cancer, which included surgery, radiation and chemotherapy. However, revolutionary treatments are now under development, and researchers are now using laboratory discoveries to design drugs that will exploit specific biological processes in cancer.

Presently bone seeking radiopharmaceuticals have proven to be a promising modality in the treatment of metastatic bone cancer, but patients require more effective radiopharmaceuticals for not only pain palliation, but also stopping the spread of this cancer. In the mission to identify those radiopharmaceuticals, ongoing research involves a trial and error approach to find the drug that will interact more effectively and selectively with the tumor. There are factors that should be taken into consideration when analyzing the radiopharmaceutical, namely the pharmacological and chemical properties of the drug. The speciation studies have shown that [^{117m}Sn]Sn(IV)-PEI-MP complexes could prove more effective in delivering antitumor effect in bone lesions, but the exact mode of action of the Sn(IV) is not known in the blood plasma. This does not limit its therapeutic usefulness and the only way to avoid, control, and counteract harmful drug effects depends on a good understanding of the mechanism involved. On the basis of this knowledge, it is possible to control the toxicity, if present, or decide whether to proceed with the administration of the drug in patients. Since the discovery that the blood plasma ligands can compete with the metal-ion *in vivo* for complexation, an effort was made to determine the binding interaction for the complexation of Cysteine and Histidine with Sn(IV) in this study. The formation constants were determined using potentiometry and a computational modeling program ESTA (Equilibrium Simulation by Titration Analysis). The

outcomes have shown that the complexation of both ligands with Sn(IV) results in the formation of hydroxyl species.

ACKNOWLEDGEMENTS

I would like to give thanks to the following:

North West University for giving me an opportunity to study, especially the Center of Applied Radiation Science and Technology (CARST) for making it possible for me to explore in this field of Nuclear Technology.
South African Nuclear Energy Corporation (Necsa) for financial support, and allowing me to use their facilities, especially the Radiochemistry department.
Ms Vuvu Msutwana-Qupe and her colleagues for a warm welcome in Necsa, you really made this place to be a cheerful working environment.
Mr Daniel Mogano for introducing me to the aspects of this project.
My supervisors David R. Jansen, Judith Wagener and Dr Jan Rijn Zeevaart for their continued assistance and guidance throughout this study, your invaluable eagerness is greatly appreciated.
My family, especially my parents and my sister Happy for their care, emotional support and their prayers throughout my studies.
All my friends, particularly Olebogeng Matshidiso, for their encouragement on registering this degree.
Special thanks to my husband Itumeleng and my son Onalenna Teddy for their patience and understanding during my studies.
Above all, Almighty God for giving me strength until I finish this work.

TABLE OF CONTENTS

LIST OF FIGURES

LIST OF TABLES

LIST OF ABBREVIATIONS

β	Overall formation constant
α	Electron transfer coefficients / alpha particle (Helium nucleus)
γ	Activity coefficient
DTPA	Diethyltriamine pentaacetic acid
Sn	The element Tin
PEI-MP	N,N,N-trimethylenephosphonate polyethyleneimine
Cys	The amino acid Cysteine
His	The amino acid Histidine
ECCLES	Evaluation of Constituent Concentration in Large Equilibrium Systems
ESTA	Equilibrium Simulation by Titration Analysis
MAb	Monoclonal antibodies
P	The element Phosphorus
Sr	The element Strontium
Sm	The element Samarium
MDP	Methylene diphosphonic acid also known as Medronate
HEDP	1-Hydroxy-ethylene-diphosphonic acid also known as Etidronate
Tc	The element Technetium
EDTMP	Ethylenediaminetetramethylenephosphonic acid
APD	1-hydroxy-3-amino-propylidene-diphosphonic acid
APDDMP	N,N-dimethylenephosphonate-1-hydroxy-3-aminopropylidene

	Diphosphonic acid
pH	Negative logarithm of the free acid concentration
E_0	Electrode constant
M	Metal or mol/dm^3
L	Ligand
H	Proton
$\bar{Z}$	Formation function; the average number of ligands bound per metal ion
$\bar{Z}_H$	Protonation formation function; the average number of protons bound per metal-ion
$\bar{Q}$	Deprotonation function; the average number of protons lost by the ligand due to complexation
$\bar{n}$	Average number of protons per ligand in the absence of metal-ion
ESTA1	Simulation module of ESTA
ESTA2A	Optimisation module of ESTA
LWL	Low molecular weight ligand
pK_a	Negative logarithm of the acid dissociation constant
HSAB	Hard Soft Acid and Base
K_w	Water dissociation constant
Log β	Logarithm of the overall formation constant

OUTLINE OF THESIS

Chapter 1 describes the study which is to characterize the binding interaction between the ligands (Cysteine and Histidine) and the metal-ion, Sn(IV). The purpose of the study is geared towards eventually establishing a blood plasma model for Sn(IV). The chapter explains the complications associated with metastatic bone cancer, which are bone pain, spinal cord compression and bone fracture and also the designing of an effective radiopharmaceutical in order to cure this disease. Some account of what has already been done in this problem area is presented in this chapter.

Theoretical background to the study is elaborated in Chapter 2, to gain more understanding of the particular problem area as well as the study design. This part describes the numerous methods that have been used for treatment of cancer, the requirements for designing a suitable radiopharmaceutical and also what has been done in the past to address this problem.

Chapter 3 explains the descriptive research design and why a particular design has been chosen. The quantitative methods for data collection and analysis have been indicated in this section.

By the use of tables, graphs and figures it was possible to report and discuss the findings in Chapter 4. This chapter describes the measurement of protonation constants for Cysteine and Histidine, also the formation constants of these ligands with Sn(IV). Chapter 5 serves to conclude and show that the research objectives were fully addressed and provides recommendations for future work.

CHAPTER 1

INTRODUCTION

1. Introduction

Cancer is a new growth of tissue resulting from a continuous proliferation of abnormal cells that have the ability to invade and destroy other tissues. This cancer which may arise from any type of cell and in any body tissue is not a single disease, but a large number of diseases classified according to the tissue and type of cell of origin. This uncontrolled growth of cells results in the formation of a tumor which is a cluster of abnormal cells. Almost all cancers form tumors, but not all tumors are cancerous, or malignant, the greatest number are benign (not threatening to health). The most significant attribute of malignant tumors is their ability to spread beyond the site of origin. They may invade neighbouring tissues by direct extension of infiltration, or it may disseminate to distant sites, forming secondary growths known as metastases. The routes and sites of metastases vary with different primary cancers. For metastatic bone cancer to occur tumor cells may migrate into the lymphatic channels and be carried to the draining lymph nodes, or they may penetrate the blood vessels. Once in the bloodstream, the tumor cells are carried to the point at which the vessels become too small for the large tumor cells to pass and therefore in this case they will be trapped in the bone. The lung and liver are common sites of metastases followed by the skeleton [1].

Metastatic bone disease being a common clinical problem accounts for 99% of all malignant tumors in bone. The occurrence of these painful bone metastases in patients with advanced cancer is high, because it results from primary cancers of the prostate, lung and breast. This disease is painful and certainly incurable if not diagnosed and treated early.

Bone pain, which is characteristic of metastatic bone cancer can reach very high levels and is a major concern in most oncology units the world over. The organ that is most likely to be affected by these metastases is the bone marrow as it contains high levels of nutrients.

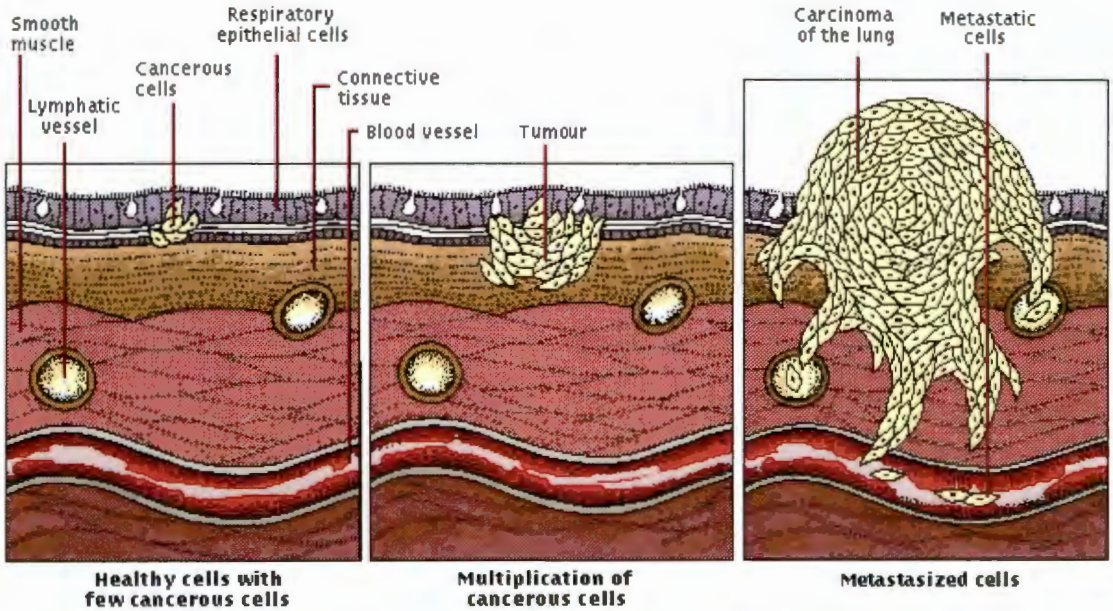

Figure 1. 1 The demonstration of how secondary tumours occur.

1.1 Symptoms of bone metastases

The symptoms of bone metastasis vary among patients. However, some patients do not have any sign that this disease exists at all. The most common symptom for bone metastasis includes hypercalcaemia of malignancy, bone pain, bone fracture and spinal cord compression.

1.1.1 Hypercalcaemia of malignancy

Hypercalcaemia causes a number of unpleasant signs and symptoms, which vary considerably from patient to patient. These are often non-specific, affecting many systems in the body, and can easily be mistaken for symptoms of the underlying cancer or associated treatment if there is no acute awareness of the possibility of hypercalcaemia. If untreated, a progressive rise in serum calcium

will occur, leading to deterioration in renal function and conscious level. Death ultimately ensues as the result of cardiac arrhythmia and renal failure [2].

1.1.2 Bone Pain

Pain is usually a presenting symptom and is caused by variety of factors including periosteal stretching, compression of infiltration of nerve roots and local effects of cytokines produced by lymphocytes. Bone metastases are commonly associated with significant pain that impairs quality of life. The pain is often at the site of the metastasis, which is referred to as localized pain.

1.1.3 Bone fracture

The bone may be affected as a result of the cancer cells spreading to the bone and these will result in a process known as osteolysis whereby parts of the bone are damaged. This may be so severe that holes also known as lytic lesions develop on the bone. These lytic lesions will weaken the bone and increase the possibility of the breakage causing severe pain to the patient.

1.1.4 Spinal Cord Compression

Cancer that has metastasized to the backbone can press on the spinal cord. Compression of the spinal cord may occur in association with spinal cord instability or in isolation. If the secondary tumor is located in the spinal area, it can result in spinal cord compression. This is one of the most serious complications of bone metastases. This can lead to back pain or make walking painful and difficult. Not only can the pressure on the spinal cord cause pain, but it can also damage the spinal cord so that the legs become numb and even paralyzed.

Bone metastases cause considerable morbidity, and the palliative and supportive treatment that sufferers require constitutes a major health care problem. Optimum management requires a multidisciplinary team including not only medical and radiation oncologists, radiologists and nuclear medicine physicians but also symptom control and terminal care specialists. In recent years there have been many exciting developments in both the understanding of the pathophysiological process involved and treatment options.

Though bone metastases can be managed, the treatment remains palliative at present. The goal of treatment is to decrease pain, prevent further bone breakdown and to restore function to patients with bone metastasis. This is done, in part, by strengthening the bone and reducing the risk of fractures. Ultimately, treatment is intended to improve the patient's quality of life. Several treatment strategies may be used to reduce pain and potentially delay progression of the bone metastases. Options for treatment include systemic radiation therapy, which is the use of radiopharmaceuticals, chemotherapy, hormone therapy and also utilizing bisphosphonates.

1.2 Background

Presently pain palliation with bone seeking radiopharmaceuticals has proven to be an effective treatment modality in patients with metastatic bone pain. The bone seeking radiopharmaceuticals are extremely powerful in treating scattered painful bone metastases, for which external beam radiotherapy is impossible because of the large field of irradiation. A radiopharmaceutical can be defined as a chemical compound containing a radionuclide intended especially for parenteral use [3]. The chemistry of radiopharmaceuticals involves the attachment or incorporation of a radionuclide to an organic molecule called a ligand. The ligand can be described as any molecule or ion that has at least one electron pair that can be donated. The ligand may also function as a Lewis base,

as they are nucleophiles. If the organic molecule has favorable medicinal and biological properties, the end product which constitutes a radioactive moiety, is called a radiopharmaceutical.

In the composition of the radiopharmaceutical, which involves a ligand and radionuclide, the ligand is usually the non-active substance and only serves as a carrier of a radionuclide to its destination. The radionuclide is the main component that works in the treatment. Its radiation will cause death in a percentage of cells within the range of the emitted decay particles, e.g. alpha, beta, Auger or conversion electrons. The decrease in tumor cells and pressure will bring relief to the patient.

Since pain palliation with bone-seeking radiopharmaceuticals is an efficient and cost effective pain management tool in patients with advanced bone cancer, bone-seeking radiopharmaceuticals have received considerable attention for the treatment of metastatic bone cancer.

Therapeutic radiopharmaceuticals are utilized on the basis of the therapeutic electron emissions of particular radionuclides, some of which may also emit imaging photons.

There are radiopharmaceuticals that are approved for the treatment of metastatic bone cancer, but they only provide pain relief. The basis for the action of these therapeutic agents is their incorporation into bone mineral and their β emission, which limits their range of action to the near neighborhood of their increased concentration in pathological areas such as metastases, where the attempt at healing by the bone results in increased uptake.

The approved radionuclides used for bone pain emit β particles, which are electrons with maximum energy between 0.01 MeV and 1.4 MeV with low tissue penetration. They do not allow for an increase in the dose without a threat to the

bone marrow in terms of radiotoxicity. For these reasons clinical research has been stimulated in order to find other radionuclides, which may have improved physical properties that permit treatment with fewer side effects on the myeloproliferative cells in the bone marrow. There is a need for a radiopharmaceutical that will not only provide pain palliation, but also serve as a means of slowing and eventually stopping the spread of metastases whilst sparing the bone marrow. In order to accomplish that improvement, the appropriate radionuclide should be used when developing radiopharmaceuticals specifically for targeting the bone where the tumor is present. Target specificity and selectivity is a crucial factor when designing the effective radiopharmaceutical. The more selective a drug for its target, the less chance that it will interact with different sites and the less chance that it will have undesired side effects. After trials that were carried out on several radionuclides, the results showed that ^{117m}Sn is an exception in that its emission consists primarily of conversion electrons of discrete energies rather than beta particles. Theoretically, it is assumed that the limited penetration of conversion electrons should reduce the absorbed dose to the bone marrow. These assumptions were also confirmed by the studies in animals that have demonstrated that ^{117m}Sn in the form of Sn(IV)-DTPA localizes selectively in the bone and appears to remain fixed with no or extremely slow release other than through physical decay [4]. The only problem with this radiopharmaceutical is that DTPA is not bone seeking.

Since ^{117m}Sn has desired properties as a suitable radionuclide for curing metastases, it was vital to pursue studies on the appropriate ligand to deliver it to its destination. The use of the water soluble polymer, N,N,N-trimethylenephosphonate-polyethyleneimine (PEI-MP) was taken into consideration. This ligand (PEI-MP) is known for its high affinity for Ca(II), which is the criterion that has to be met when developing therapeutic agents for metastatic bone cancer.

Recent studies were conducted to determine the formation constants for the complexation of PEI-MP with Sn(IV) [5] and the outcome showed that reasonable deposition and accumulation in bone can be expected. However, the compound with the best binding interactions is not necessarily the best drug to use in medicine, and some of the most active drugs discovered *in vitro* show no activity at all *in vivo*. This is because a clinically useful drug has to travel through the body to reach its target. There could be possible barriers and hurdles that would prevent a drug from reaching its target and, as far as the drugs are concerned, it is a long, strenuous, and dangerous journey. Studies have shown that when the radiopharmaceutical is injected intravenously, it is exposed to a wide variety of ligands and metal-ions in the blood plasma. These blood plasma ligands can affect the speciation of the radiopharmaceutical in the body by having a high affinity for the radio-metal, or the metal-ions in the body can displace the radio-metal, and this poses a threat to the survival of the radiopharmaceutical before reaching its destination [5].

Therefore these findings are not sufficient for the complex, Sn(IV)-PEI-MP to be declared an effective drug. The *in vivo* behaviour of the complex, Sn(IV)-PEI-MP, should be known before it can be administered to the patient. This study is part of the attempt to be able to have a model that can monitor the *in vivo* behaviour of proposed Sn(IV) based radiopharmaceuticals before they can be administered to human beings. It is possible that the outcome of such modeling will be that there is incomplete localization of the radiopharmaceutical to the targeted site, meaning that there will be no selective uptake of radiopharmaceutical into the bone.

Since the research has proved that the polymeric ligand, PEI-MP can be effective in delivering Sn(II) to bone and have an anti-tumor effect, Sn(IV) is also considered and its study will be beneficial to broaden our understanding of the behaviour of these Sn-ligand systems in blood plasma.

One can imagine the radiopharmaceutical entering the body to interact with the target, which is the bone, to fight the metastases. Since this radio-drug is a complex of a radionuclide and a ligand, and its behaviour in the body is not known, it is impossible to understand its long-term fate or survival. Therefore before any predictions can be made pertaining to the *in vivo* performance of Sn(IV)-PEI-MP, its biodistribution and long-term fate in the blood plasma should be investigated. It is important to broaden our understanding of the behaviour of Sn(IV) in blood plasma taking into consideration the competition for complexation from *in vivo* metal-ions and ligands. In general, the aim is to design drugs which will survive long enough in blood plasma to locate selectively at the site of bone metastasis and adhere there until the desired effect has been realised.

The focus of this study is to characterize the behaviour of Sn(IV) within the blood plasma to determine the binding interactions of this metal-ion with a variety of blood plasma ligands. The two ligands that are to be studied are building blocks of proteins that are termed amino acids.

Proteins are large biomolecules that occur in every living organism. There are many types of proteins with various biological functions. Regardless of their appearances and functions, they are chemically similar. They are made up of many amino acid units linked together by amide bonds in a long chain. Amino acids constitute an important class of nitrogen-containing, naturally occurring compounds. The composition of amino acids includes amino groups and carboxylic groups. Since amino acids contain both acidic and basic groups in the same molecule they undergo an internal acid-base reaction and exist primarily in the form of a dipolar ion, or zwitterion. Amino acid zwitterions are like internal salts and have many of the physical characteristics associated with inorganic salts. Thus, amino acids are crystalline, have high melting points, and are soluble in water but insoluble in hydrocarbons. In addition, amino acids are amphoteric: they can either react as acids or as bases, depending on the circumstances. In aqueous acid solution, the amino acid zwitterion accepts a proton to yield a

cation, and in aqueous basic solution the zwitterions lose a proton to form an anion [6].

The biological function of amino acids is that they are constituent monomer units from which the biopolymers based on the peptide bond are built. The two particular amino acids that are studied are Cysteine and Histidine. Cysteine is a neutral amino acid with a hydrophilic side chain whereas Histidine is a ligand with a basic amino group in its side chain.

Histidine is an imidazole, and it plays an essential role in biological systems as a ligand. The imidazole moiety of the histidyl residue in a large number of metalloproteins forms all or part of the binding site of many transition metal-ions. It is also known that the imidazolate anion acts as a bridging ligand in certain metalloenzymes [7].

The results obtained after characterizing its binding interactions will be included in the ECCLES database (Evaluation of Constituent Concentration in Large Equilibrium Systems) for modeling, which will make it possible to better predict the behaviour of Sn(IV)- and thereby minimize animal experiments. This involves a series of calculations on model metal-ion complexes to gain insights into understanding the observed ligand-metal-ion specificities. The specificities include preferred coordination numbers, relative affinity for the various possible protein supplied ligands, and the preferred binding orientation.

1.3 Research Objectives

Currently a trial and error approach is adopted in ongoing clinical research to find suitable and effective treatments for bone metastases. The drug that is designed to be target orientated aims to modify the lead compound (radiopharmaceutical)

such that it interacts more effectively and selectively with its molecular target (bone) in the body. Stronger drug-target interactions should increase the activity of the drug while an increase in target selectivity will lower side effects. Therefore to effectively understand the behaviour of the radionuclide within the blood plasma the factors affecting its action have to be taken into consideration, which are the competition of blood plasma ligands for complexation. In this case speciation experiments can assist in explaining the behaviour of the radiopharmaceutical. The speciation model can be used to predict the behaviour of an administered radiopharmaceutical and deduce whether it will survive in the blood plasma and, with no liver and kidney uptake, that it will migrate to its destination.

The purpose of this project is to generate the stability constants for Sn(IV) with a variety of ligands typically found in blood plasma. This will contribute towards establishing a blood plasma model for Sn(IV) using ECCLES to make predictions about the behaviour of the bone seeking radiopharmaceutical *in vivo*. It will be possible to see if the drug can withstand the conditions in the body and be delivered to the targeted site, the bone tumor.

The experiments were performed using glass electrode potentiometry. The titration data were collected and analysed (with ESTA) to identify the various complexes formed. Their stability constants were determined for Sn(IV) with the blood plasma ligands, Cysteine and Histidine.

The main aim of this study is to determine:

- protonation constants for Cysteine and Histidine
- possible complexes that are formed by Cysteine and Histidine with Sn(IV) and
- stability constants using the ESTA set of programs

his h Histidin **cys** c Cystein

Figure 1.2 Molecular structures of the blood plasma ligands studied

CHAPTER 2

THEORETICAL BACKGROUND

2. Theoretical background

2.1 Therapy of cancer in bone

While bone metastases can be difficult to live with, there are many therapeutic options available for alleviating pain and treating the cancer itself. Cancer pain management is multidisciplinary in approach so there is no universal or singular modality of treatment.

Different treatment strategies have been considered primarily as agents to provide pain palliation in far advanced metastases involving bone. The requirements for achieving this purpose are rather modest. It is not necessary to obtain much tumor regression and it is desirable to avoid significant toxicity. These treatments include: chemotherapy, bisphosphonates, surgery and radiation therapy (external beam and targeted radioisotope therapy).

2.1.1 Chemotherapy

Chemotherapy is the use of drugs in the treatment of cancer. Since a drug is distributed throughout the body by the bloodstream, chemotherapy is prescribed for tumours that have spread beyond the area accessible by surgery or radiotherapy. Chemotherapy is commonly used for palliation. The two major problems limiting the usefulness of chemotherapy are toxicity and resistance. Toxicity of chemotherapy can be distressing but can be minimized by the use of modern medicine, dosage modifications and careful explanation of the intended treatment. It is not suitable for all patients but, when used appropriately, can produce very worthwhile palliation of symptoms without causing unacceptable toxicity. This is because the chemotherapeutic agents are not effective in the rapidly growing cancer cells; they have very serious side effects.

It is being found that chemotherapy can be hazardous in patients with extensive bone disease due to poor bone marrow tolerance following replacement of functioning marrow by tumor and the effects of previous irradiation. [8]

2.1.2 Bisphosphonates

Bisphosphonates form part of standard therapy for hypercalcemia and the prevention of skeletal events in some cancers. Bisphosphonates are a class of drugs that prevents the breakdown or resorption of bone. In the last decade, bisphosphonates were regularly used to treat osteoporosis and bone pain from diseases such as metastatic breast cancer and multiple myeloma, a cancer that starts in the bone marrow. These drugs help reduce bone pain, slow down bone damage caused by the cancer, reduce high blood calcium levels, and lower the risk of broken bones. They are more effective when x-rays shows the metastatic cancer is causing the bone to become thinner and weaker. They are effective in treating osteoblastic metastases. [2]

2.1.2.1 Bisphosphonates in tumor cells

Bisphosphonates have become the treatment of choice for hypercalcemia of malignancy and osteolytic bone diseases associated with tumor metastases. In addition to decreasing hypercalcemia and the subsequent risk of fractures, bisphosphonates can reduce bone pain.

In animal models of metastatic disease, bisphosphonates can slow the development of bone metastases and reduce tumor burden, apparently by an indirect effect through inhibition of osteoclast activity, thus preventing the release of tumor-stimulating growth factors. Until recently there is no evidence that bisphosphonates can affect tumors directly *in vivo* but it was found that pamidronate and incadronate could cause cell cycle arrest and apoptosis of human myeloma cell lines *in vitro* that could potentially be achieved in the close

vicinity of resorbing osteoclasts [2]. Because myeloma cells are known to be closely associated with sites of bone resorption, this raises the possibility that bisphosphonates could have direct antitumor effects on myeloma cells *in vivo*. It has been recently found that bisphosphonates bound to bone mineral also inhibit the adhesion and spreading of breast carcinoma cells to bone. It was postulated that further studies are required to establish whether beneficial effects occur *in vivo*, because this advocates greatly the use of bisphosphonates to prevent the development of metastatic bone lesions [9]. These bisphosphonates require chronic administration over long periods to be effective. Contraindications include sensitivity to phosphates.

2.1.3 Surgery

The principal approach to curing cancer is to remove all the malignant cells by a surgical operation. In the past this meant the removal of all the involved tissue and as much potentially involved tissue as possible, including adjacent tissue and lymph nodes. At times, many cancers, though, are at too advanced a stage at the time of diagnosis to be eradicated by surgery. If local extension involves neighbouring tissue that cannot be sacrificed, or if distant metastases are already present, surgery will not cure the cancer. Even when it is clear that surgical cure is not possible, however, surgery may help to relieve symptoms, such as obstruction, or to reduce the size of the tumour in an effort to improve the patient's response to subsequent radiotherapy or chemotherapy [8].

2.1.4 Radiation therapy for the palliation of bone metastases

Although pain is now more aggressively managed than in the past, poorly controlled pain syndromes, associated with significant reductions in quality of life, remain an ongoing clinical dilemma [10]. Radiation therapy has been regarded

as an effective palliative treatment for incurable cancer. Radiation can be used to palliate pain, bleeding or obstruction.

Radiation therapy is based on the fact that normal tissues have a greater ability to recover from the effects of radiation than do tumour cells. Thus, a radiation dose sufficient to destroy tumour cells will only temporarily injure adjacent normal cells.

2.1.4.1 External beam radiotherapy

Localized external beam radiotherapy is the treatment of choice for the palliation of painful single sites. However, for the treatment of multiple involved sites, wide field irradiation such as hemibody treatment is a rational alternative to sequential treatments with standard fields.

2.1.4.2 Targeted radioisotope therapy

An alternative approach to the relief of multifocal bone pain is the systemic administration of a radionuclide, which concentrates at sites of increased bone turnover. Bone metastases from breast cancer will excite an osteoblastic response in bone, leading to an increased uptake of the radiopharmaceutical. In this way, therapeutic doses of radionuclides may be localized close to the tumor, by utilizing uptake mechanisms in adjacent non-tumor tissue. Bone-seeking radiopharmaceuticals have traditionally been used to image tumors in bone, but depending on the carrier ligand and the energy of the radioactive label, these agents can also be used to treat primary or metastatic tumors in bone [11].

The therapeutic use of radioactive label tracer molecules is currently an area of considerable interest and research. Targeted radiotherapy has several theoretical advantages over external beam radiotherapy. Firstly, the intracellular uptake of therapeutic radiopharmaceuticals ensures that the radiation dose is

delivered specifically to the tumor, and normal tissues are spared unnecessary irradiation, allowing repeated treatments if necessary. Secondly, given an adequate blood supply, the radiation dose should be evenly administered throughout the treatment volume. The α- or β- emitting radionuclides were the most suitable, but they have been expensive and technically difficult to produce, so that despite the theoretical attractions of radioisotope therapy, only relatively few have been evaluated clinically [2].

The success of treatment depends upon matching the known biochemical and physiological characteristics of the target tissue to the optimal radionuclide and pharmaceutical carrier. Important considerations governing the selection of an individual radionuclide include particle range, physical half life, gamma yield and chemistry.

2.2. Physical and Chemical Properties of Radionuclide Therapy

As more radionuclide therapies move from laboratory feasibility studies into clinical reality, it becomes increasingly important for the labeling chemistry to produce consistently a stable radiopharmaceutical that remains intact under the challenge of human catabolism. Similarly, once proof of principle is established to bring a radionuclide conjugate into clinical therapy trials, dosimetric estimates should be made to select the appropriate radionuclide properties, which are based on animal specific or patient-specific pharmacokinetics and match a set of specific clinical endpoints. These properties may include the radionuclide physical half-life, radiolabeled conjugate biological uptake and clearance, product specific activity, range and type of emissions, and resultant effects on tumor and normal tissue cellular survival.

2.2.1 Desirable Radionuclide Characteristics

It is essential that the half-life of a radionuclide used in radionuclide therapy is compatible with the rates of localization in target tissues and clearance of the carrier molecules from normal tissues. The proper choice of half-life for a radionuclide therapy agent has implications on the dose delivered to both target and normal tissue, the dose rate, the feasibility of multidose treatment regimes, and in some cases the widespread availability of the agent.

Another factor to consider with relevance to radionuclide selection for radionuclide therapy is what happens to the radionuclide when the carrier protein is catabolized, either at the tumor site or in normal tissues. Particularly important are the localization and clearance characteristics of radionuclide therapy agents in non-target tissues, since production of radiotoxic side effects in these tissues will limit the activity that can be administered to patients. Studies have shown that for radiometals the nature of the bifunctional chelator can also have a significant effect on the rate at which the radionuclide is cleared. Thus, if the monoclonal antibodies (MAb) to be used for radionuclide therapy are known to be internalized, the rate of that process must be slow relative to the half-life of the radionuclide in order to maximize the radiation dose to the tumor. Increasing clearance of activity from normal tissues can markedly reduce radiation doses to those organs and to other normal tissues as long as the catabolized form of the radionuclide does not redistribute to other radiosensitive non-target tissues [12].

There are several radionuclides with a spectrum of chemical and physical properties currently available. These and others form the basis for designing and formulating more sophisticated therapeutic radiopharmaceuticals for treatment of bone metastasis.

The interest in application of radionuclides to therapy of bone malignancies, particularly for palliative relief of bone pain, is not new, but has recently undergone renewal.

A number of complexations of ligands and metal-ions has been performed in order to develop an effective radiopharmaceutical for palliation of metastatic bone cancer. Some of these agents have shown good efficacy in relieving bone pain secondary to bone metastases, and others are still under investigation.

2.3 Approved radiopharmaceuticals for palliation of metastatic bone cancer

The three approved radiopharmaceuticals used to treat metastatic bone pain are sodium phosphate (^{32}P), strontium chloride (^{89}Sr) and samarium (^{153}Sm) lexidronam.

^{32}P was one of the first radionuclides used in the treatment of bone metastases. It has a physical half-life of 14.3 days and decays by ß-emission to ^{32}S. The maximum β -energy is 1.71 MeV with a mean energy of 0.695 MeV. This agent may be imaged with a moderate success using the bremsstrahlung emission [8].

Originally it was believed that its effect was mainly from incorporation into the tumor itself. However the tumor to non-tumor ratio is not favorable and the relief of pain is primarily because of its uptake into bone mineral and not the tumor. Similar to ^{89}Sr, ^{32}P has a high beta emission and has no accompanying gamma photon, making monitoring somewhat difficult. ^{32}P was significantly associated with hematological toxicities.

^{89}Sr is a pure beta-emitting radioisotope, a chemical analogue of calcium, and it is therefore avidly concentrated by areas of high osteoblastic activity. Selective uptake and prolonged retention at sites of increased bone mineral turnover

provide precise bone lesions targeting. The radioactive emission of ^{89}Sr commercialized as Metastron poses very little radioprotection concerns. Overall studies show pain relief in up to 80% patients of which 10 to 40% became effectively pain free. Upon administration of Metastron, the only reported toxicity is temporary myelosuppression [8]. The main problem with this radionuclide is it long half-life of 50 days which gives problems in clinical practice from a radioactive waste management perspective.

^{153}Sm is reactor produced in high radionuclidic purity by neutron bombardment of enriched ^{152}Sm oxide. Complexed with the chelator ethylene-di-aminetetramethylenephosphonate (EDTMP), it is supplied as ^{153}Sm-lexidronam. ^{153}Sm decays with emissions of both β and γ- particles.

Satisfactory results were obtained using ^{153}Sm-EDTMP supplied as Quadramet in the pain palliation therapy of patients suffering from this form of cancer [8]. The active ingredient of this radiopharmaceutical has a short half-life of 1.9 days and this can be advantageous in that it is easier to administer repeated doses. The ECCLES program was used to illustrate the *in vivo* behavior of the ^{153}Sm-EDTMP, and the results were closely comparable to the clinical observations [13,14]. At high levels of administered ^{153}Sm, an increase in survival of patients with metastatic prostate cancer was demonstrated, but at the cost of severe myelotoxicity.

^{186}Re, which is produced by irradiating enriched ^{185}Re, is chemically similar to ^{99m}Tc. It can be readily complexed with HEDP with a relatively high radionuclide and radiochemical purity. HEDP also known as Etidronate has higher bone uptake than MDP [15]. It has been used as ^{99m}Tc(Sn)-HEDP. ^{186}Re(Sn)-HEDP particularly has shown favourable biodistribution and dosimetry, and has been approved for clinical use [16,17]. The active ingredient of ^{186}Re-HEDP has a half life compound or ^{186}Re of 3.7 days and decays by the emission of a β–particle with energy of 1.07 MeV and a γ-particle emission of 137 keV (9% abundance).

In addition, it has been reported that ^{188}Re-HEDP was labelled with the radiochemical purity higher than 99% and it demonstrated an in-vivo behaviour similar to that of ^{99m}Tc-HEDP with a clearance of 70% within 6 hours [16].

2.4 Radiopharmaceuticals investigated for palliation of metastatic bone cancer

Focus has been on the experimental bone-localizing therapeutic radiopharmaceuticals in the pursuit for a cure of metastatic bone cancer. ECCLES capacity was used in the research leading to the improvement of ^{153}Sm-EDTMP by not only providing pain relief, but also suppressing and regressing bone metastases and even osteosarcomas. The ^{153}Sm was replaced with ^{166}Ho because it emits higher beta energy compared to Sm, but the results were not satisfactory. The model revealed that although there is only a log K of 0.5 difference between the formation constant for Sm(III) vs Ho(III) with EDTMP, Ho(III) is competed for by citrate to such an extend that a substantial percentage of the injected Ho(III) will complex to it in the blood plasma causing the Ho(III) not to be delivered solely to bone as intended. [12].

The decision was taken to replace this ligand with another that will deliver a high percentage of injected ^{166}Ho to bone tumors. The ligand that was used was supposed to accumulate in regions of high Ca(II) concentration, which is characteristic of areas affected by secondary bone metastasis. Bisphosphonates were tried as ligands because of their properties, in which they have high affinity for calcium, inhibit the osteoclasts and are a cure for osteoporosis. Attempts were made with [1-hydroxyethylidene]-disphosphonic acid (HEDP) and methylenediphosphonic acid (MDP) as ligands complexed to lanthanides, Sm and Ho [18]. HEDP, also known as Etidronate has been extensively studied and used in bone imaging in the form of [^{99m}Tc]Sn-HEDP before [15].

After the blood plasma model had been constructed for these two ligands with the metal-ions in the blood plasma, it was found that HEDP has a higher specific bone uptake than MDP possibly due to the presence of the hydroxy group on HEDP. But the overall results were that they are not good carriers of the lanthanide ions because of preferential Ca(II) complexation, and the plasma mobilization index shows that zinc will be mobilized [19]. 1-hydroxy-3-amino-propilydenediphosphonic acid (APD) was also studied because it has pain palliation properties. It was found that neutral species formed (MLH) with lanthanides investigated and that colloid formation is possible, which will result in liver uptake. ECCLES also predicted high liver uptake [20].

Since APD exhibits a high affinity for calcium, the ligand was modified by adding two charged methylenephosphonate groups at the primary amine center, resulting in the synthesis of N,N,-dimethylenephosphonate-1-hydroxy-4-aminopropylidene-diphosphonate (APDDMP) to prevent formation of the neutral species with high liver uptake.

The newly designed ligand was complexed to trivalent metal-ions, ^{153}Sm and ^{166}Ho. Blood plasma modeling predicted that ^{166}Ho-APDDMP complex will have little liver or bone uptake while ^{153}Sm-APDDMP had a moderate bone uptake. Clinical observations also verified no liver uptake and low bone uptake [21].

Since ^{153}Sm and ^{166}Ho emit high-energy beta radiation, which do not allow for an increase in the administered radiation dose without posing a threat to bone marrow in terms of radiotoxicity, a more suitable radionuclide has to be identified. The nature of the emissions (β, internal conversion, or Auger electrons) determines the therapeutic suitability of the radionuclide, because the range of penetration is related to the energy of the electrons. ^{117m}Sn has favorable radionuclidic properties which makes it an attractive candidate for clinical and research applications in nuclear medicine [4]. Firstly, it could be useful as a biological tracer for tin metabolism and for developing tin-labelled

radiopharmaceuticals for diagnostic purposes, particularly for applications requiring delayed imaging or long-term quantitative studies. Secondly, tin can be used as a radiotherapeutic agent owing to the abundance of Auger and low energy conversion-electron emissions in its decay. Other properties are emissions with minimal toxicity to the bone marrow, a half-life of 13.6 days, and also tin itself is considered as bone seeking [22]. These characteristics make it possible to increase the administered dose with minimal toxicity to the patient.
Since studies have shown that ^{117m}Sn exhibit desirable properties as an agent for radionuclide therapy, it was complexed to the APDDMP ligand. ^{117m}Sn was investigated, because of its potentially low bone marrow radio toxicity, which means that it could perform as a highly effective radiopharmaceutical in pain palliation compared to ^{153}Sm and ^{166}Ho, and also in curative treatment of bone metastasis. After the blood plasma models were constructed using the computer code ECCLES and the results compared with those gathered from tests on a rodent model, it was found that Sn(II)-APDDMP complex has only some liver and bone uptake although a higher trabecular to normal bone ratio was recorded. The prediction from the speciation calculation showed that it is because of the high affinity of APDDMP for Ca(II), causing some of the Sn(II)-APDDMP complex to dissociate. Sn(II) preferentially forms complexes with histidinate or cysteinate in blood plasma. This dissociation and formation of the above complexes resulted in high bladder uptake as well as high kidney uptake and excretion [23].

Water-soluble polymers were studied as potential drug carriers, exploiting the enhanced permeability and retention (EPR) effect, where macromolecules passively accumulate in solid tumors. The phenomenon is thought to be caused by the production of compounds such as Vascular Permeability Factor (VPF) and Bradykinine in tumor cells that increase vascular permeability of the tumor tissue. Retention is enhanced by the impairment of the lymphatic system in tumor tissue, retarding the removal of macromolecules from tumors. The polymer must therefore be large enough not to be taken up in healthy tissue but not so large to be trapped in organs such as the liver or kidneys. The assumption that it has

potential to deliver therapeutic radionuclides to tumors was made because of its design. To extend the approach to therapeutic radiopharmaceuticals, the water-soluble polymer, polyethyleneimine was functionalized with methylene-phosphonate groups to make the resulting water-soluble polymer, PEI-MP, bone seeking.

Studies were undertaken to evaluate whether the polymer has the potential to selectively deliver the therapeutic radionuclide to tumors. Pre-clinical work using ^{99m}Tc-labelled PEI-MP showed uptake in healthy bone, kidneys or liver depending on the size of the polymer. Formation constants were generated with the blood plasma metal- ions to predict the behaviour of this ligand *in vivo*. The results show that PEI-MP has strong affinity for Ca(II) and Mg(II). The good bone uptake of ^{99m}Tc- PEI-MP showed that the ligand tends to have less leakage from healthy vascular tissue into healthy bone than other bisphosphonates ligands, because of the EPR effect [24].

Further studies were conducted using the form of tin; Sn(II). The research was done by Zeevaart *et al* [25] where Sn(II) was complexed to PEI-MP since ^{117m}Sn has appropriate radiation properties and PEI-MP has selective bone tumors uptake into the bone tumors. The study described the speciation of Sn(II)-PEI-MP and other known ^{117}Sn(II) containing radiopharmaceuticals in blood plasma. Other ligands were DTPA, HEDP, Cysteine and Histidine (blood plasma ligands). [5] After the model was constructed it was predicted that Sn(II) will remain bound to the polymer and have only slight reticuloendothelial uptake. The preliminary primate studies indeed proved that the complex between Sn(II) and PEI-MP remains intact in blood plasma. It was found that the competition for the radionuclide by the blood plasma ligands is low and between 87.1% and 82.8% of the complex survives in blood plasma which is then available for bone localization. In the animal studies good bone uptake was found with baboons for 3-8 kDa fractions (small polymer size that acts as a bisphosphonate and no EPR effect is experienced). For Sn(II)-DTPA and Sn(II)-HEDP lower bone uptake,

slow blood clearance and liver uptake was predicted and were reported in the literature [25].

The scope of these studies changed and Sn(IV) is now also considered as a potential chemical form for delivering ^{117m}Sn to the target. The complexation of the Sn(IV) to two modified ligands APDDMP and PEI-MP [5] was studied. Sn(IV)-PEI-MP complexation showed that the ligand forms relatively stable complexes with Sn(IV) which could possibly survive the conditions of blood plasma. The complexes that form at pH 7.4 are less diverse than with APDDMP, and because the Sn(IV)-PEI-MP shows promising results, it is vital to have an insight into the *in vivo* behaviour of the prospective radiopharmaceutical. Due to good bone-seeking capabilities of the PEI-MP, reasonable deposition and accumulation of Sn(IV)-PEI-MP in bone can be expected. However, the influence of the other blood plasma metal ions on the complex is unknown which requires further studies. In order to describe these phenomena one needs to set-up a blood plasma model of Sn(IV). Therefore it is important to gain an insight into the interaction of Sn(IV) in the blood plasma to make predictions of the behaviour of Sn(IV) in blood plasma. This effort consists of finding the formation constants for all the low molecular weight ligands (40 in total i.e amino acids) in blood plasma with Sn(IV). No constants are available in literature and therefore a number of constants need to be measured to have a basis to deduce the rest using LFER relationships.

Once a Sn(IV) blood plasma model has been drawn up the Sn(IV) PEI-MP complex can be inserted at the proposed concentrations and, as with the Sn(II) blood plasma model, one can determine the fate of the complex.

2.5 Potentiometry: A Technique for determining stability constants

Potentiometry is the most widely used technique to measure the formation constants that are required. The crux of this method is measurement of the e.m.f.

between a hydrogen ion-sensitive electrode and a suitable reference electrode immersed in an experimental solution under investigation [26]. When the metal-ions and the ligands are placed in a given system competition takes place and the complexes with the highest formation constants survive. The chemical interaction between the two – described by formation constants, needs to be measured in order to calculate this. In this case, the electrodes are used to measure the voltages that provide chemical information.
Potentiometry measures the electrical potential developed by an electrode in an electrolyte solution at zero current.

In the simplest case, the analyte participates in the chemistry of a galvanic cell. Imagine a solution containing an electro-active species (the analyte) whose activity (concentration) we wish to measure. An electro-active species is one that can donate or accept electrons from an electrode. In potentiometry the measuring setup always consists of two electrodes: the measuring electrode, and the reference electrode. Both the electrodes are half cells. We can turn the unknown into a half-cell by inserting an electrode into the solution to transfer the electrons to or from the analyte. Because this electrode responds directly to the analyte, it is called the indicator electrode. The second half-cell has a fixed composition so that it will have a constant potential. Because of this constant potential, the second half-cell is called a reference electrode. When these two electrodes are placed in a solution together they produce a certain potential. Depending on the construction of the half cells, the potential produced is the sum of several individual potentials. Potential-determining transitions always occur at the phase boundaries, e.g. between the solution and the electrode surface. The cell voltage is the difference between the variable potentials that responds to analyte activity and the constant potential of the reference electrode [27]. The electrodes develop potential that depends on the activities of the species present; therefore there is a requirement of the use of a relatively large excess of a background inert electrolyte.

The electrode potential for a half reaction depends upon the driving force for the half reaction. Thus, from the Le Chatelier principle, it is to be expected that electrode potentials are concentration dependent. The relationship between electrode potential and concentration of electrode species was first enunciated in the nineteenth century by a German chemist by the name of Nernst, his name is attached to this important relationship.

Consider the generalized half-reaction

$aA + bB + \ldots ne^- \leftrightarrow cC + dD + \ldots$ (2.5.a)

Where the capital letters (A, B, C, D) represent molecular species of the reacting species, e^- represents the electron, and the lower case (a, b, c, d) indicate the number of moles of each species (including electrons) participating in the half-cell reaction. According to the Nernst equation, the electrode potential E for this reaction is given by

$$E = E^0 - \frac{RT}{nF} \log \frac{[C]^c [D]^d}{[A]^a [B]^b} \qquad (2.5.b)$$

where the E^0 is a constant called the standard electrode potential.

At room temperature (298 K), the collection of constants in front of the logarithm has units of joules per coulomb or volts. That is,

$RT/nF = 8.316 \text{ J mol}^{-1} \text{ deg}^{-1} \times 298 \text{ deg} / n \text{ equiv mol}^{-1} \times 96491 \text{ C equiv}^{-1}$

$= 2.568 \times 10^{-2} \text{ J C}^{-1} / n$

$= 2.568 \times 10^{-2} \text{ V} / n$

Upon converting the natural logarithm to a base ten (by multiplication by 2.303), the foregoing equation becomes at room temperature

$$E = E^0 - \frac{0.0591}{n} \log \frac{[C]^c [D]^d}{[A]^a [B]^b} \qquad (2.5.c)$$

To summarize the meaning of the bracketed terms in the above equation,

when the substance A is a gas,

[A] = partial pressure in atmospheres

when A is a solute

[A] = Activity, $a_A \approx M_A$

when A is a pure liquid in excess, or the solvent, [A] is constant and is included in the constant E^0. Formally, then,

[A] = 1.00

Application of the Nernst equation is illustrated in the following examples:

$Zn^{2+} + 2e^- \rightleftharpoons Zn(s)$ $$E = E^0 - \frac{0.0591}{2}\log\frac{1}{[Zn^{2+}]}$$ (2.5 d)

$Fe^{3+} + e^- \rightleftharpoons Fe^{2+}$ $$E = E^0 - \frac{0.0591}{1}\log\frac{[Fe^{2+}]}{[Fe^{3+}]}$$ (2.5.e)

$2H^+ + 2e^- \rightleftharpoons H_2(g)$ $$E = E^0 - \frac{0.0591}{2}\log\frac{p_{H_2}}{[H^+]^2}$$ (2.5.f)

In this example, p_{H_2} represents the partial pressure of hydrogen, expressed in atmospheres, at the surface of the electrode. Usually p_{H_2} will be very close to atmospheric pressure.

The potentials of cells encountered in the laboratory are affected by several other sources, one of them being liquid junction. Any time two dissimilar electrolyte solutions are in contact, a voltage difference develops at their interface and is called liquid junction potentian. This small voltage (usually a few millivolts) is found at each end of a salt bridge connecting two half-cells. The junction potential puts a fundamental limitation on the accuracy of direct potentiometric measurements, because the contribution of the junction to the measured voltage is not usually known [28].

Although different types of hydrogen ion-sensitive electrodes, such as hydrogen gas electrode and the quinhydrone electrode have been used in the past, nowadays virtually all pH-metrically determined formation constants are obtained with the use of the glass electrode. This can be attributed not only to convenience and robustness but also to the high quality and reliability of modern glass electrodes.

The glass electrode used is a typical pH combination electrode, incorporating both glass and reference electrode in one body, used to measure the pH. Ideally, an ion-selective electrode responds only to one intended ion and is unaffected by other species. In practice, there is always some of interference by other ions. Ion-selective electrodes are fundamentally different from metal electrodes in that ion-selective electrodes do not depend on redox processes. The key feature of an ideal ion-selective electrode is a thin membrane across which only the intended ion can migrate.

From the cell potential, which is measured as a function of a titrant volume by the electrode, dissociation and formation constants of the complexes can be calculated, considering the thermodynamic equilibrium that occurs.

2.5.1 Formation constants of complexes in biological fluids

Formation constants have important applications in the area of metal-ion interactions with low-molar-mass ligands. The term, formation constant, is a special name for the equilibrium constant of a metal complex formation reaction in solution. These may be written generally as

$pM + qL + rH \rightleftharpoons M_pL_qH_r$

where

M = a metal-ion species

L = a ligand

H = hydrogen ions

p, q, r = the stoichiometric coefficients of the reactants, r may be positive or negative, if negative the implication is that protons are removed or that hydroxide ligands are added.

When a given metal species, M, interacts with a given ligand, L, in general, several competing reactions takes place concomitantly, corresponding to several sets of values of the stoichiometric coefficients, p, q and r. Thus, in general, several complexes, each with its own distinctive stoichiometry, are formed and co-exist in equilibrium.

The thermodynamic stability can be indicated by an equilibrium constant relating its concentration to the concentration of other species when the system has reached equilibrium. The stability of a complex in solution refers to the degree of association between the two species involved in the state of equilibrium. Qualitatively, the greater the association of the two, the greater the stability of the compound. The magnitude of the equilibrium constant for the association, quantitatively expresses the stability. Thus, if we have a reaction of the type:

$M + 4L \rightleftharpoons ML_4$

then the larger the stability constant, the higher the proportion of ML_4 that exists in the solution. Free metal-ions rarely exist in solution so that M, will usually be surrounded by solvent molecules which will compete with the ligand molecules, L, and be successively replaced by them. For simplicity, generally these solvent molecules are ignored and the stability constants are written as follows,

$$M + L \rightleftharpoons ML \qquad K_1 = \frac{[ML]}{[M][L]}$$

$$ML + L \rightleftharpoons ML_2 \qquad K_2 = \frac{[ML_2]}{[ML][L]}$$

where K_1 and K_2 are referred to as stepwise stability constants.

Another way of expressing the equilibrium relations is by the overall formation constant

$M + L \rightleftharpoons ML$ $\qquad \beta_1 = \frac{[ML]}{[M][L]}$

$M + 2L \rightleftharpoons ML_2$ $\qquad \beta_2 = \frac{[ML_2]}{[M][L]^2}$

The formation constant β for the equilibrium of complex formation is defined as follows:

$$\beta_{pqr} = \frac{[M_p L_q H_r]}{[M]^p [L]^q [H]^r} \qquad (2.5\ g)$$

for the reaction $pM + qL + rH \rightleftharpoons M_pL_qH_r$

where p=0 the protonation constant is used to describe the equilibria.

There is a relationship between K_is (stepwise formation constants for stability constants) and β_is (overall formation constants).

Generally, there is a slowly descending progression in the values of the K_is in any particular system. Thus, typically, as the ligand is added to the solution of metal-ions, ML is first formed before any other complex in the series. As addition of ligand is continued, the ML_2 concentration rises rapidly, while the ML concentration drops, then ML_3 becomes dominant until the highest complex ML_N is formed to the nearly complete exclusion of all others at very high ligand concentrations.

There are several reasons for a steady decrease in K_i values as the number of ligands increases:

1. Statistical factors.
2. Increased steric hindrance as the number of ligands increases if they are bulkier than the H_2O molecules they replace.

3. Coulombic factors, mainly in complexes with charged ligands.

In so far as formation constants are used in constructing speciation models of biological fluids, a question arises regarding the validity of assuming biological fluids to be at equilibrium. Perrin and Agarwal [29] point out that a biological system is never truly in a state of equilibrium but they justify the assumption of equilibrium as a first approximation because to achieve high efficiencies of energy conversion, most biological systems operate near to reversible equilibria.

In applying formation constants to speciation calculations, close attention needs to be given to certain points. First, the value of a stoichiometric formation constant generally depends on the ionic strength of the solutions in which the constant is determined, and also on the identity of the ionic medium in which the reacting system is investigated.

The second point is that in fitting experimental data different researchers may propose differing chemical models as best fitting their respective experimental data. The differences in general tend to affect the identities of the minor complex species, usually there is agreement on the identities of the major species although the values of the formation constants of the latter may vary somewhat from one chemical model or set of experimental conditions, to another [30].

In applying a formation constant to a given speciation modelling problem, it is of paramount importance to ensure that the constant has been measured under conditions which correspond as closely as possible to the ionic composition, reactant concentration ranges, temperature etc. of the biological fluid under consideration.

The potentiometric data obtained can be analyzed by using the set of software programs called Equilibrium Simulation by Titration Analysis (ESTA).

2.6 Chemical speciation and modelling

Chemical speciation is a term used to denote all of the different physico-chemical forms and associated concentrations in which a given metal-ion or ligand can exist in dynamic equilibrium in a given aqueous system.

According to Letkeman, chemists have for many years, used the concept of effective or conditional stability constant in order to predict the ability of ligands to complex metal-ions *in vivo* [31]. It has been realized that the ability of ligands to bind to metal-ions depends on the pH and concentration of both the ligand and the metal. However, until recently the calculations were too time-consuming, and it took the arrival of fast personal computers and appropriate software to make these calculations possible hence the application of chemical speciation and modeling.

Chemical speciation describes the composition, i.e. types and concentration of chemical compounds of an aqueous solution, and in this case blood plasma. The significance of chemical speciation lies in its usefulness as a tool for the interpretation of chemodynamic properties and toxicity of chemical compounds.

When the metal-ion, for example Sn(IV), is injected into the blood plasma, it can exist in a wide variety of chemical forms, such as free ion (Sn^{4+}), hydroxo complex e.g. $[Sn(OH)]^{3+}$, chelate complexes with organic ligands, and also sorbed on particles. Because the most toxic species is the free ion, we need to know how much of it is present to assess the potential risk of reticuloendothelial uptake [32].

Chemical speciation depends, amongst other factors, on the composition of the system, pH, temperature, ionic strength, and time, where the system is assumed to be in thermodynamic equilibrium. It can be determined experimentally or be estimated computationally. In practice, chemical speciation calculations are used

to estimate concentration of species that are difficult or impossible to measure. Calculations are performed using specialized computer programs to obtain estimates of unknown concentrations based on experimental information and equilibrium constants [33].

Computer simulation of equilibrium systems is becoming increasingly capable of providing useful information concerning speciation. The general requirements of such a study are the total concentrations (or free concentrations, if available) of all components and the formation constants of complexes formed from the components. A prior prediction of extent of complexation cannot merely be based on the size of formation constants so computer programs that can solve large systems of non-linear equations have been developed [34].

The schematic diagram of the constituents of a chemical speciation model is shown in figure 2.1 below. This study was confined to the determination constants as not enough constants have been gathered yet to complete the Sn(IV) blood plasma model.

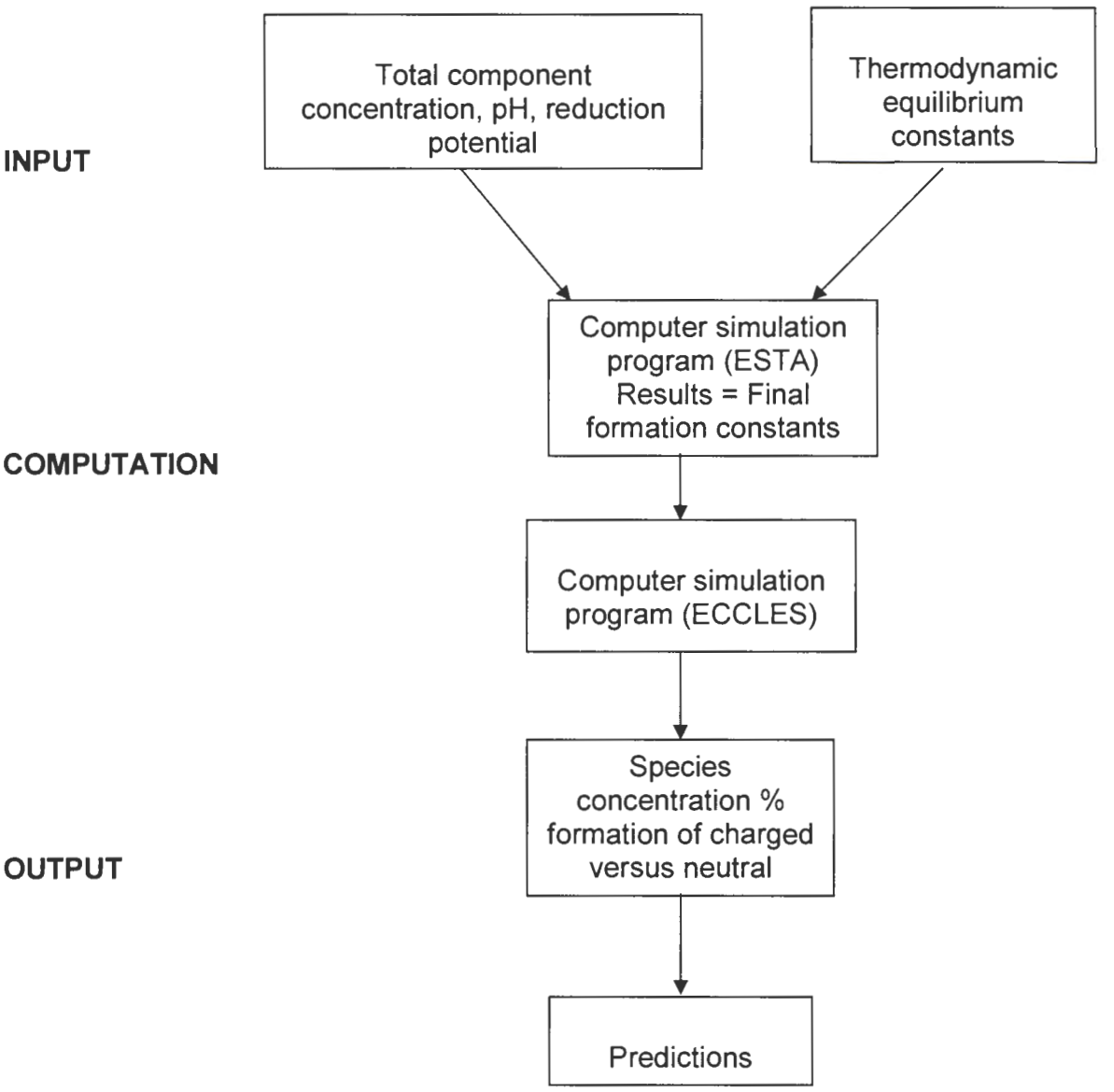

Figure 2. 1 The basic components of a chemical speciation model.

2.6.1 ESTA

The titration data from potentiometry is refined and analysed by the use of ESTA (Equilibrium Simulation by Titration Analysis) [35, 36]. This library of programs is used for simulating simple equilibrium distributions of chemical species. ESTA works by imposing the conditions of the mass balance equation (m.b.e.) in the standard way by equating the calculated concentration (T_i^c) with the real (analytical) concentration ($T^r{}_i$).

$T_i^r = T_i^c, \ldots \ _i = 1$ NC (2.6.1a)

where

T_i^r = real total concentration

T_i^c = calculated total concentration

NC = number of components appearing in complex

i = general index for components

$$T_i^c = [X_i] + \sum_{j=1}^{NJ} r_{ji} \Gamma_j \beta_j \prod_{n=1}^{NC} [X_n]^{r_{jn}} \qquad (2.6.1b)$$

$$T_i^r = \frac{C_i^v V^0 + \sum_{m=1}^{NB} C_{im}^B v_m}{V^0 + \sum_{m=1}^{NB} v_m} \qquad (2.6.1c)$$

$$\Gamma_j = \left(\prod_{n=1}^{NC} \gamma_n^{rjn} \right) \Big/ \gamma_j \qquad (2.6.1d)$$

Where $[X_i]$ is the free concentration of component *i*

There should always be free concentrations known in potentiometry, which is obtained from the experimentally determined emf. This emf is linked to the activity of the electrode ion by ESTA.

In general, the equation relating the potential of an electrode to the activity of the electrode ion can be written in the form

$$E_k = E_k^0 + E_k^{is} + E_k^{LJ} \quad k = 1,2,3.....n \qquad (2.6.1e)$$

Where E_k^0 is the electrode response intercept, E_k^{is} the electrode selectivity, E_k^{LJ} the liquid junction.

For the purpose of formation-constant determination, E_k^{is} is usually given by

$$E_k^{is} = s_k \log\{X_k\} = s_k \log\gamma_k + s_k \log[X_k] \qquad (2.6.1f)$$

Unlike some other programs, ESTA accommodates the well-known effects of interfering ions.

The effects of interfering ions are accounted for by the Eisenman equation.

$$E_k^{is} = S_k \log\left[\{X_k\}^{1/\alpha} + \sum_i \left(K_i \{X_i\}^{z_k/z_i}\right)^{1/\alpha}\right]^{\alpha} \qquad (2.6.1g)$$

The liquid- junction term E_k^{LJ} is not taken constant but is derived from the Henderson equation

$$E_k^{LJ'} = -(RT/F)\ln(1 + d[X_H]/I) \qquad (2.6.1h)$$

where I is the concentration of the background univalent electrolyte. This is used to correct for the liquid junction potential changes in the calibration of the glass electrode.

The Henderson equation is used in the prediction of the potential across junctions of various electrolytes at the constant ionic strength

$$E_k^{LJ'} = \frac{-RT}{F} \times \frac{\sum_i \gamma_i^s \{S_i^s\} - \lambda_i^b \{S_i^b\}}{\sum_i z_i \left(\lambda_i^s \{S_i^s\} - \lambda_i^b \{S_i^b\}\right)} \times \ln \frac{\sum_i \lambda_i^s z_i \{S_i^s\}}{\sum_i \lambda_i^b z_i \{S_i^b\}} \qquad (2.6.1i)$$

The Debye-Huckel formula is used to calculate the activity coefficients.

$$-\log\gamma = \frac{Az^2\sqrt{I}}{1 + Ba\sqrt{I}} + cI \qquad (2.6.1j)$$

Converting into thermodynamics constants, equations (2.6.1b, g and h) require thermodynamic values of the parameters $\beta_j, E_k^0, K_{ki}\lambda_i^s$ and λ_i^b, those that are defined with respect to a standard state based on reactions occurring at infinite dilution in water at zero ionic strength. However, it is established practice to work with conditional constants $\beta_j, E_k^0, K_{ki}\lambda_i^s$ and λ_i^b, which refer to some or other ionic strength(I). The formation constants reported are conditional formation constants characterized by the medium in which they were determined. Such constants can be converted into the corresponding thermodynamic values:

$$\beta_j = {}^I\beta_j / {}^I\Gamma_j$$

and this changes equation 2.6.1g into

$$E_k^{IS} = S_k \log^1 \gamma_k + S_k \log\left\{ [X_k]^{1/\alpha} + \sum_i \left(\frac{K_{ki}\left({}^I\gamma_i [X_i]^{z_k/z_i}\right)}{{}^I\gamma_k} \right)^{1/\alpha} \right\}^{\alpha} \qquad (2.6.1\ k)$$

These parameters are converted into thermodynamic values as follows:

$$E_k^0 = {}^I E_k^0 - S_k \log {}^I\gamma_k$$

$$K_{ki} = {}^I K_{ki}\left({}^I\gamma_k / \left({}^I\gamma_i\right)^{z_k/z_i}\right)$$

$$\lambda_i^s = {}^I\lambda_i^s / {}^I\gamma_i^s, \qquad \lambda_i^b = {}^I\lambda_b^i / {}^I\gamma_i^b$$

Thermodynamic formation constants, β, and unknown free concentration can be calculated from other free concentrations and parameters that have been experimentally determined from the electrode equations.

The NC mass balance equations can in principle be solved for any unknowns as long as all remaining parameters are known. In particular, there are NC free concentrations that can be determined. On the other hand, if one of the free

concentrations has been measured experimentally, the remaining free concentrations and one other parameter (such as v_m, β_j, C_i^v, C_{im}^B, or T_i^r) can be calculated. Consequently, the procedures for solution of the m.b.e. fall into two categories. In the first, these equations are solved for NC free concentrations without any reference to the electrode equation. The electrode potential can subsequently be obtained by substitution into other equations. In the second category, it is necessary to solve the electrode equation to obtain the free electrode-ion concentration before solving the m.b.e. Solving the electrode equation for $[X_k]$ requires knowledge of all the free concentrations so it is necessary to implement an iterative solution of this equation and the m.b.e.

A Newton-Raphson procedure is generally the most efficient way to solve the mass balance equations. The equation can be set up in terms of the absolute values of unknowns except for the free concentration $[X_k]$ and the formation constants for which natural logarithms are convenient. The second method can be used to solve the equations for free concentration only when the Newton-Raphson fails .

2.6.1.1 Initial estimates

It is well known that the efficiency of the Newton-Raphson method is considerably improved if good initial estimates can be obtained for the unknowns. Here, there are two classes of unknowns to consider. The first consists of the free concentrations of the components. Unless such concentrations can be obtained from electrode equations, they are very difficult to estimate. Secondly, there are those unknowns which are experimental parameters such as total titrant, titrant concentrations, and titration volumes. Formation constants can also be included in this class. Generally it is possible to estimate reasonable initial values.

Gauss-Newton algorithms are used to optimize a calculated model representation of the experimental data. This is done by calculating from the experimental value the initial concentration of the participating species and formation constants at the first and second titrations.

Electrode potentials are available and initial estimates of the corresponding free electrode-ion concentration can therefore be calculated. Initial estimates of all parameters at the third and each subsequent point of a titration are best obtained by linear extrapolation of the solution from the previous two points based on the change in electrode potential.

Standard deviations of the parameters and the Hamilton R-factor, which gives the indication of the difference of the objective function that has been minimized and the experimental data points, can be calculated when the estimates of parameters being refined are judged to be sufficiently close to the solution. In contrast, the Hamilton R-limit only takes the total number of data points into account and therefore gives a theoretical minimum of the R-factor. The closer the R-factor is to the R-limit the better the calculated parameters fit the measured data.

The advantage of ESTA is that it accommodates chemical systems of up to 10 components forming up to 99 complexes. Titrations involving up to three electrodes and three burettes are permitted. The program can take into account variations in ionic strength and the associated changes in activity coefficients. They also permit corrections of titration data affected by liquid-junction potentials and imperfect ion-selectivity of electrodes.

The ESTA library of programs contains modules that perform more kinds of calculations. These are ESTA1, which is the simulation module, and ESTA2, which is the optimization module.

2.6.1.1 (a) ESTA1: simulation module

ESTA1 can determine the single values for almost any titration parameter point-by-point. The calculations fall into two categories: species-distribution calculations and potentiometric titrations calculations. The latter includes determination of emf values, formation constants estimates, total analytical concentrations, initial vessel concentrations and initial burette concentrations. Other kinds of titration analyses are also possible, like calculation of appropriate weights, an overall objective function value and the relative contribution of the most important errors based on errors in both emf and total concentrations (task OBJE and OBJT respectively).

In this case it is useful in the generation of formation function values, i.e. formation function values (task ZBAR) and deprotonation function values (task QBAR).

2.6.1.2 Formation functions

$\bar{Z}_H$ and $\bar{n}$ are the formation functions for the protonated ligands. $\bar{Z}_H$ is defined as the average number of protons bound per ligand, while $\bar{n}$ is described as the average number of protons per ligand in the absence of the metal.

$$\bar{Z}_H = [bound\ H] / L_T \qquad (2.6.1\ i)$$

$$[bound\ H] = H_T - H + [OH]$$
$$= H_T - H + K_W H^{-1} \qquad (2.6.1\ j)$$

where OH^- = hydroxide ion

K_W = dissociation constant of water

So, $\bar{Z}_H = \left(H_T - H - K_W H^{-1}\right) / L_T$ (2.6.1 k)

H_T and L_T are known from analytically determined concentrations and K_W is usually known from the literature. Since H is measured by the glass electrode, $\bar{Z}_H$ can be calculated at a number of pH values. It will then be possible for the protonation curve to be plotted.

And

$$\bar{n} = \left(H^* - H = K_W H^{-1}\right) / L_T^r \quad (2.6.1\ l)$$

Thus an average proton stoichiometric coefficient $\bar{r}$ may be calculated for any given M and L stoichiometry. The assumption is made here that the complex is predominant.

$\bar{Z}$ is the formation function for metal-ligand systems, and can be described as the number of ligands bound per metal-ion at a certain pH value.

It is given by

$$\bar{Z} = [L\ bound\ to\ M_T] / M_T \quad (2.6.1.m)$$

$$= \left(L_T - [bound\ H]\ \bar{Z}_H\right) / M_T$$

$$= \left(L_T - \{H_T - H + K_W H^{-1}\} / \bar{Z}_H\right) / M_T \quad (2.6.1.n)$$

where $\bar{Z}_H$ is defined in equation 2.6.1.n. Therefore, protonation formation constants for the ligand must be determined before $\bar{Z}$ can be calculated from observed experimental points.

2.6.1.3 Deprotonation function

The deprotonation function $\bar{Q}$, describes the number of protons lost by the ligand during complexation at respective pH-values. Essentially, it gives the displacement of protons by the metal-ion(s) during complex formation. The function is given by

$$\overline{Q} = \frac{T_H^* - T_H}{T_M} \qquad (2.6.1.o)$$

where T_H and T_M are the total proton and metal concentrations respectively. T_H^* depicts the calculated concentration of protons that would result in the observed pH if no complexation occurred.

By using this program, graphs can be drawn of pH vs. $\overline{Z}_H$ or $\overline{Q}$ and $\overline{Z}$ vs. pA, where the observed and calculated functions can be compared and E_k^{obs}, E_k^{calc} evaluated respectively. If the calculated and observed curves match each other closely in the pH region of interest, the proposed model and formation constants can be accepted. $\overline{n}$ is used together with $\overline{Q}$ to confirm species like MLOH(MLH_{-1}) at high pH values.

A file of simulated titration data, with a format identical to ESTA input, can be generated as output.

2.6.1.3 (a) ESTA2: the optimization modules

There are two optimization programs: ESTA2A and ESTA2B, differing only in the way weights are calculated. They can only be used when it is needed to determine, for one or more parameters, the best values based on a least-squares procedure applied to a whole system of titrations. It is used to refine the following parameters: formation constants, vessel and burette concentration, electrode slope and initial vessel volume. It is possible to group together, over any combination of titrations, local parameters of the same type and the same value so that they are refined together as a single parameter. The objective functions may be weighted or unweighted. The sum of squares of residuals may be minimized with respect to either emf-task OBJE or total concentrations – task OBJT.

The total number of titrations is dimensioned to 20 and the total number of points to 1000 but these can readily be varied if necessary. A file of titration data containing the optimized parameter values and with a format identical to ESTA input can be generated as output.

In the estimation of the formation constants which are extracted from the primary data, there are questions that always arise which are fundamental to any model-fitting process and ESTA should always be able to answer them at the end of analysis. Some of the questions are;

- When is the fitted model "correct"?
- What is a "good" fit to the data?
- How does one or more species improve the fit?

Clearly the answers to these questions are dependent upon the quality of the data, overall goodness-of-fit, and the statistics for the best model.

Because the potentiometric data and ESTA analysis provides a good idea of how the complexation of a ligand and metal-ion will behave without the competition by the blood plasma ligands and metal-ions, it is essential to investigate in order to make accurate predictions about the behaviour of the complex *in vivo*. The computer program ECCLES [37] predicts the speciation of metal-ions or ligands in biological fluids such as blood plasma. ECCLES stands for **E**valuation of **C**onstituent **C**oncentrations in **L**arge **E**quilibrium **S**ystems and simulates the nature of the metal-ion binding to low-molecular-weight ligands (LWL) in human blood plasma because these play an important role in biological systems. The distribution of Ca^{II}, Mg^{II}, Mn^{II}, Fe^{III}, Cu^{I}, Cu^{II}, Ni^{II}, Zn^{II} and Pb^{II} among 5 000 complexes formed with 40 or more ligands is computed. Binary and ternary complexes (such as ML_1L_2 and $ML_1L_2L_3$, where L_1, L_2 and L_3 are different ligands binding to the same metal-ion) are also taken into account.

CHAPTER 3

EXPERIMENTAL

3. Experimental

3.1 Reagents

The two ligands, L-Cysteine hydrochloride anhydrous (F.W.=157.62 g) was bought from Fluka, and L-Histidine (F.W.=155.16 g) was obtained from Merck Chemicals (Pty) Ltd and used as received. The metal salt tin(IV) chloride pentahydrate ($SnCl_4.5H_2O$, F.W. 350.58 g, purity 98%) was obtained from Aldrich. Fresh metal-ion solutions were employed in the titrations. The solutions were made by dissolving the reagent grade chloride salt in a 0.1 M acid solution in order to prevent hydrolysis. No further purification was made to the salt. Sodium hydroxide (NaOH, F.W.40.00 g and purity 99%) and sodium Chloride (NaCl, F.W.58.44 g and purity of 99.5%) were obtained from Merck Chemicals. Hydrochloric acid (HCl, F.W. 36.46 g, 32%) used for solutions was obtained from Merck Chemicals (South Africa). De-ionized water that was used in the preparation of solutions was obtained by passing distilled water through a Milli-Q-water purification system (Millipore, Bedford, MA, USA).

3.2. Preparation of solutions

The stock solutions of 0.14 M Cysteine, 0.15 M Histidine and 0.005 M Sn(IV) were prepared. All the solutions were prepared in such a way to maintain the ionic strength of 0.15 M in the titration vessel. A standard solution of 0.15 M NaCl required for background electrolyte adjustment was prepared.

Several attempts were made to standardize the Sn(IV) solution but they were not fruitful. The idea was to get the exact concentration of Sn(IV) since it hydrolyzes, which results in the formation of a precipitate. Since there was no method that worked, the concentration used for tin was taken as it is ignoring precipitation. The titration points where precipitation occurred were omitted.

3.3. Potentiometric studies or measurements

Potentiometric titrations were performed using a Tim865 Titration Manager from Radiometer Analytical with a Metrohm 665 Dosimat and a combination glass electrode with Ag|AgCl as a reference electrode. The experimental solution was contained in the jacketed, sealed glass titration vessel. Thermostatically controlled water from the water bath at 25°C was circulated through the reaction vessel. High purity nitrogen gas was bubbled through the test solution during the entire duration of the experiments to protect the solution from atmospheric oxygen and carbon dioxide. The composition of the experimental solution was adjusted in a series of steps by adding an appropriate titrant from a burette in 0.10 ml aliquots of 0.050 M NaOH in 0.10 M NaCl. All titrations were performed beginning at a low and ending at a high pH. All solutions were held at a constant ionic strength of 0.15 M NaCl, which was used as background electrolyte because it is effectively inert. Figure 3.1 provides a schematic diagram of the titration set-up.

The combination glass electrode was calibrated regularly using strong acid-base titration data. Calibration always included a check of the measuring electrode. A reality that had to be taken into account is that glass electrodes have a variable life span and once deterioration sets in, the e.m.f. readings can no longer be relied upon. Therefore, it was necessary to check the performance of the electrode system at reasonably frequent intervals. Calibration buffers were used for this check because they have a medium acid-base concentration and their ionic strength is approximately that of the most common samples.

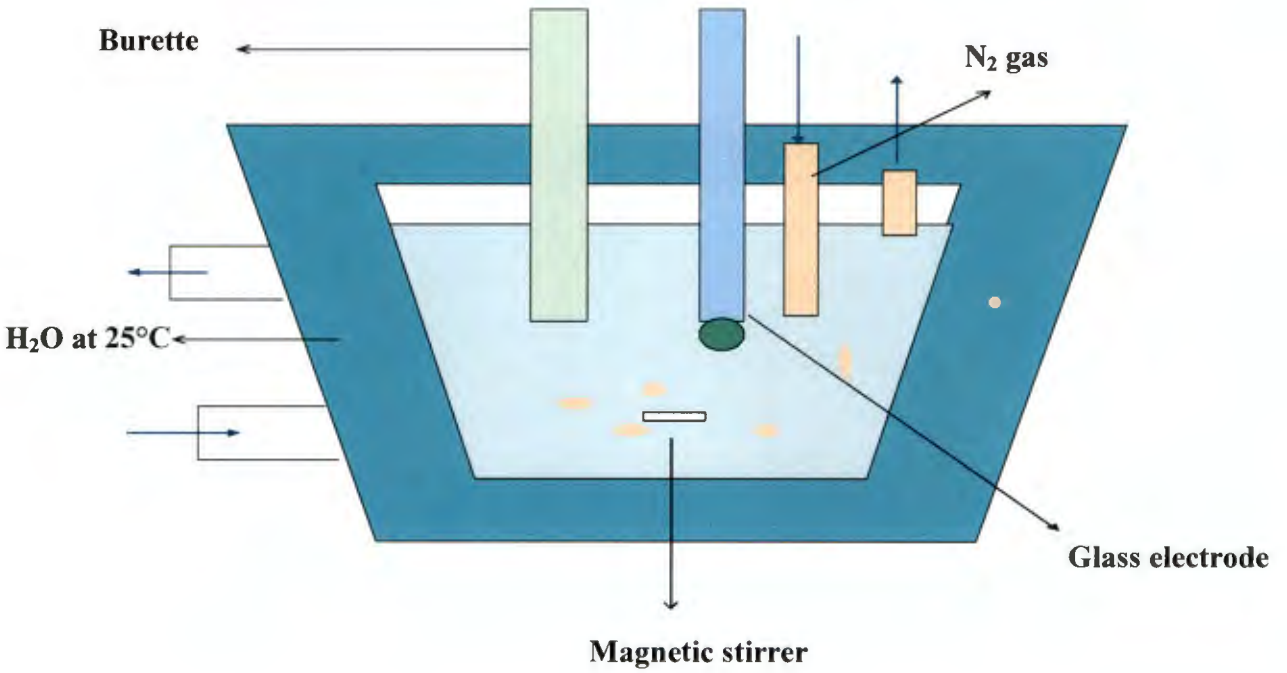

Figure 3.1 The schematic diagram of potentiometric titrations

3.4 Experimental procedures

3.4.1 Procedure for titration of Cysteine and Histidine systems

To obtain the protonation constants for the two ligands, Cysteine ($HSCH_2CH(NH_2)$ COOH.HCl) and Histidine ($C_6H_9N_3O_2$), three titrations of the ligand in the presence of various HCl concentrations were performed. First, for every titration, the calculation of E^0 and response slope of the glass electrode was performed. The emf was measured between a hydrogen ion sensitive electrode and a suitable reference electrode (combined in one electrode) immersed in the experimental solution under investigation. The measured emf was used to obtain the concentration of free hydrogen ions in the experimental

solution. The latter, obtained for a series of experimental solutions were combined with the known total analytical concentrations of metal-ion, ligand and hydrogen ions in the solution to obtain values of formation constants. The information about the electrode condition was provided by the electrode slope, electrode zero point, response time of the signal and its streaming dependency. This calculation involved the addition of 0.05 M NaOH in 0.1 M NaCl to the vessel containing various quantities of 0.05 M HCl in 0.10 M NaCl.

To determine the possible complexes present for the ligand, the titrations involved titrating varying quantities of 0.01 M Cysteine in 0.14 M NaCl, 0.01 M Histidine in 0.15 M NaCl, and 0.05 M HCl in 0.1 M NaCl with 0.05 M NaOH in 0.1 M NaCl. The pipettes used were calibrated to obtain the exact volume. From these titrations, data obtained were used to calculate the protonation constants of the ligands.

In a second series of experiments, the metal complexes were investigated. The experimental solution contained the ligand, metal-ion and acid. In all the titrations care was taken that both the titrant and titrating solution were of 0.15 M strength of chloride. This ensures an equivalent of 0.15 M NaCl at all times so as to simulate blood plasma.

Some amino acids can be identified by their titration curves. Potentiometric data make it possible to determine accurately the endpoints or inflections during titrimetric experiments by observing the titration curve. A titration curve is a plot of the pH of a solution as a function of added equivalents of hydroxide ion. As hydroxide ion is added to an aqueous solution of the fully protonated form of an amino acid, the pH increases, and the hydroxide ion removes protons from the solution by reacting with them to form water. The increase in pH flattens out when OH^- can remove a proton from an ionizable group of the amino acid rather than from the solvent. When all the protons of the ionizable group are removed, the pH again increases. The pH at the midpoint of the flattened-out region, the inflection point, is equal to the pKa of the ionizable group.

3.4.2 Specifications of the preparation of the samples for the different ligand ratios.

To establish the formation constants for the metal-ligand complexes, five titrations of different ratios were also performed, i.e. Sn(IV)-Cysteine and Sn(IV) - Histidine. The compositions of the titration solutions are listed in Tables 3.1 and 3.2

Table 3.1 Composition of experimental solutions titration of Cysteine and Histidine, respectively

0.01 M Ligand in NaCl[#] (ml)	0.05 M HCl in 0.1 M NaCl (ml)	0.15 M NaCl (ml)
4.925	10	25
6.918	10	20
9.944	10	20

[#]Where Ligand = Cysteine in 0.14 M NaCl, or Histidine in 0.15 M NaCl.

Table 3.2 Composition of experimental solutions titration of Cysteine and Histidine with Sn(IV) respectively

M:L Ratios	0.01 M Ligand in 0.1 M NaCl (ml)	0.005 Sn(IV) in 0.1 M HCl (ml)	0.15 M NaCl (ml)
1:1	1.864	3.423	19.75
1:2	3.423	3.423	18.00
1:3	5.175	3.423	16.25
1:1.5	1.114	3.423	20.5
2:1	0.875	3.423	21.00

[#]Where Ligand = Cysteine in 0.14 M NaCl, or Histidine in 0.15 M NaCl.

Although standard 2, 5 and 1 ml pipettes were used these were calibrated using a mass balance. The corrected volumes are given.

All the titrations were closely monitored for possible formation of a precipitate. Precipitation was observed at certain pH values and those points were omitted. Metal-ligand stability constants were then calculated from the titration data at five different metal to ligand concentration ratios. Data were analyzed by the computer program ESTA.

3.5 Titration data analysis (ESTA studies)

During the analysis the previously determined protonation constants were held constant. The hydrolysis constants and pK_w were taken from literature [38] and held constant during optimization procedures. Models were considered plausible if Hamilton R-factors and standard deviations of log β values were low. Where more than one model was plausible, the modeled data were compared to experimental data using the deprotonation function, $\overline{Q}$ (the average number of protons released as a result of complexation per metal-ion) or the protonation formation function, $\overline{Z}_H$ (the average number of protons per ligand). The models giving rise to the best fit of the calculated to the experimental data were considered the most plausible and reported here.

CHAPTER 4

RESULTS AND DISCUSSION

4. Results and discussion

4.1 Speciation of Cysteine with Sn(IV)

4.1.1 Proton-ligand formation constants

The protonation constants for Cysteine are presented in the table below. These are average values for titrations at different H: L ratios and are performed at 25°C at the ionic strength of 0.15 M NaCl

Table 4.1: The Protonation constants for Cysteine

Cation Species	Equilibrium	log K	Literature [18]	Hamilton R-factor
H^+	$H + L \rightleftharpoons HL$	10.28 (0.01)	10.26	0.00732
	$H + HL \rightleftharpoons H_2L$	8.15 (0.01)	8.18	
	$H + H_2L \rightleftharpoons H_3L$	1.45 (0.01)	1.65	

The protonation constants given in the table above (Table 4.1) are considered in more detail in order to gain more information about the general properties of the ligand in aqueous media.

The protonation constants obtained are compared with results of the pK_a values obtained in the literature [18] and they closely correspond to each other. These protonation constants for Cysteine were used in the modeling of the Sn(IV)-Cysteine.

The three protonation constants observed are as expected for the Cysteine ligand. According to its structure, it is evident that it is a tridentate ligand as it has three coordination sites which are –COOH, -SH and $–NH_2$.

At the beginning of the titrations, where the initial pH of the solution is set to 1.7, the solution is more acidic. Cysteine's structure has a carboxylic acid and amine. The amino group in all amino acids has a pair of non-bonding electrons, which are available for combination with the proton. Due to this, it has been observed that at lower pH, the amino group remains protonated. Increasing the pH of the solution by adding a base made it possible for the proton to dissociate. The ligand exists in protonated form while the pH of the solution exceeds the pK_a of the most acidic of the groups in the amino acids which in this case was the carboxylic acid group with pK_a = 1.71. A convenient way to describe the relative acidity of this compound is to arrange it according to pK_a, and using the Henderson-Hasselbalch equation to understand the acid-base properties of this amino acid. The Henderson-Hasselbalch equation describes that when the pH of the solution is equal to the pK_a of the compound that undergoes dissociation the concentration of the compound in its acidic form will equal the concentration of the compound in the basic form.

The carboxylic acid group loses a proton and exists in the basic form and this can be attributed to the fact that the pH of the solution has an effect on the structure of an organic compound. The thiol group of Cysteine is a weak acid with a pK_a of 8.4. At a neutral pH, a low percentage of the thiol group will be ionized. As more NaOH is added to the solution the amino group starts to dissociate. The protonation scheme for Cysteine is shown in the figure below.

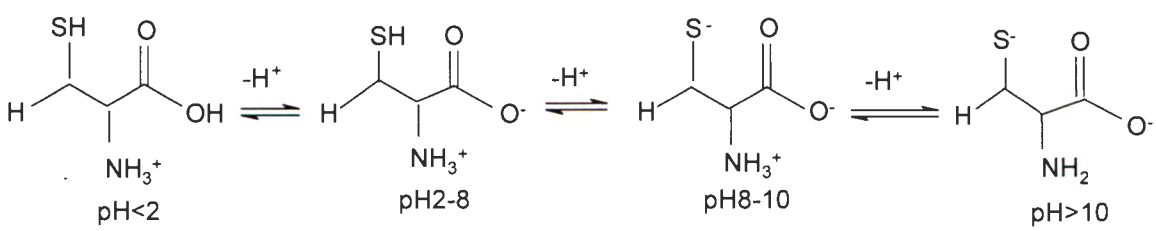

Figure 4.1 Proposed protonation scheme for Cysteine at different pH values

The way the Cysteine ligand dissociates and its protonation constants can be rationalized by comparing it with the ionization of the amino acids, lysine and methionine. The order in which the ionizable groups of the lysine and methionine loose protons is according to their pK_a's [39]. Methionine, unlike Cysteine, has a sulfur group which is not highly nucleophilic, although it will react with some electrophilic centers. It is generally not a participant in the covalent chemistry that occurs in the active centers of enzymes. The protons lost from methionine are from the carboxylic acid and the amino group (figure 4.3).

Lysine, although it does not have a thiol group, has three stability constants obtained under the same conditions as those for Cysteine. It can be seen that the first proton dissociate from the carboxyl group and the last two protons are due to the loss from the amine sites (figure 4.2). Although the two protonation constants of Cysteine pK_1 = 10.28 and pK_2 = 8.15 are higher than those of lysine pK_1 = 9.84 and pK_2 = 6.67, and methionine pKa_1 = 9.2 and pKa_2 = 2.3, they are still consistent with them.

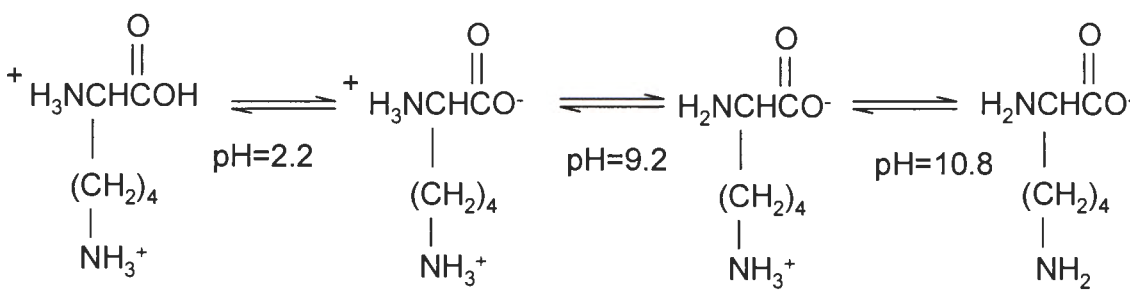

Figure 4.2 Protonation scheme for lysine

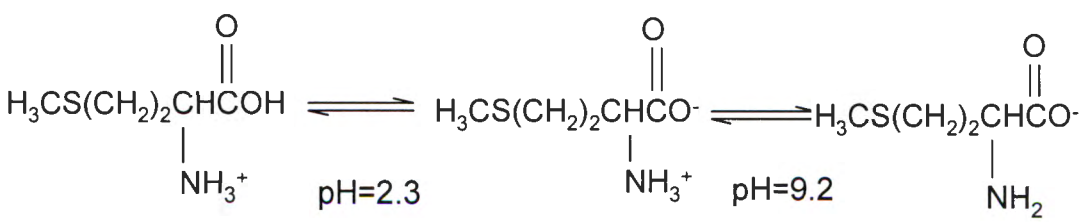

Figure 4.3 Protonation scheme for methionine at certain pH values

Protonation formation curves for Cysteine are given in Figure 4.4.

The protonation curves for the three titrations show good fits as indicated by the low Hamilton R-factor and standard deviations. The experimental data, represented by points and the calculated curves represented by a solid line, match each other very closely over the entire pH range.

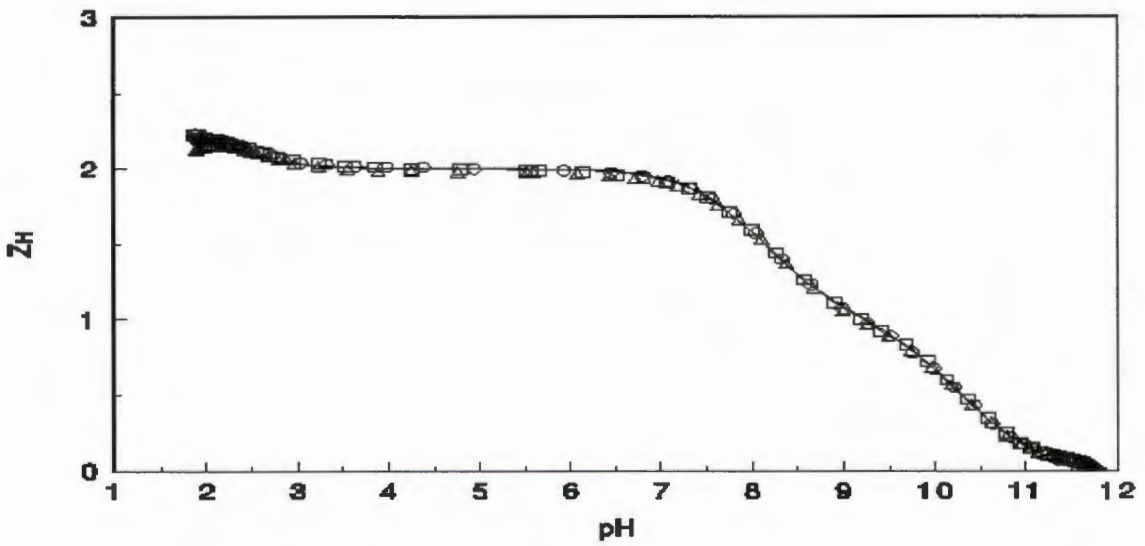

Figure 4.4 The protonation curve studied for Cysteine

Experimental (points) and modeled (lines) protonation formation curves for Cysteine. The three separate titration are represented by (O) 0.0012 M Cysteine and 0.0125 M HCl, (Δ) 0.0018 M Cysteine and 0.0135 M HCl, (□) 0.0025 M Cysteine and 0.0125 M HCl. All solutions were at 25^{0}C and 0.15 M NaCl.

According to the protonation curves it is also evident that there are three protonation constants involved. This is supported by the curves wherein below pH 2 the graph tends towards $\overline{Z}_H$ = 3, indicating that three protons have been added to Cysteine. The reason for the poor fit in this region is because the glass electrode becomes insensitive at low pH values. The graph flattens off at zero in the region of pH 10 indicating that the ligand has become fully deprotonated. At the pH of about 3, the ligand loses a proton and $\overline{Z}_H$ = 2 at pH values of 4 to 7.

This indicates that LH_2 is the dominant form of the ligand. The loss of a proton is due to the dissociation at the amino group and the pK_2 is 8.15. Another proton is lost at pH 7.3 and this dissociation was not expected so soon because the pH of the solution is still less than the pK_a of the thiol group. In this region the dominating species is the LH. When the pH of the solution increases, becoming strongly basic another proton is lost from the amino group and both groups exists in the basic form. The $\bar{Z}_H$ curve shows a slight inflection until it reaches the pH of 10 where the last proton has dissociated. This protonation indicates that the constant L is the dominant form of species at high pH and LH_2 at low pH.

Figure 4.5 below shows how the species are distributed. The inflections observed in the protonation curve correspond well with the formation of the various species involved in the model.

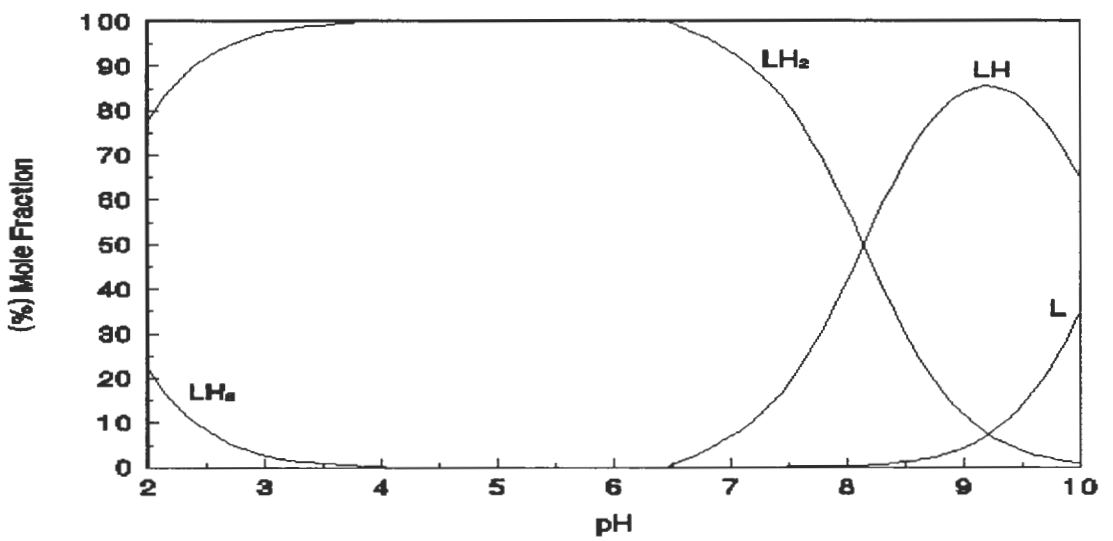

Figure 4.5 The species distribution curve for the protonation of Cysteine at 25°C and 0.15 M NaCl

All protons are lost beyond pH 10, and only the free ligand species remains. At pH 2 the LH_3 species constitute 20% of the total ligand concentration.

At pH 7.4, which is of interest in the blood plasma, the principal species formed is LH_2 and comprises 80 % of the ligand. In the same pH range there is a formation of LH (20%). At pH 10, 35% of the free ligand has already formed.

4.1.2 Complexation of Sn(IV)-Cysteine

4.1.2.1 Potentiometric formation constants for Sn(IV)-Cysteine

Table 4.2: The stability constants for Cysteine with Sn(IV) at 0.15 M (NaCl) at 25°C

Equilibrium species #	log β	Hamilton R-Factor
$Sn^{IV} + OH \rightleftharpoons SnOH$	-1.94*	0.06324
$Sn^{IV} + 6\ OH \rightleftharpoons Sn^{IV}(OH)_6$	-24.11*	
$Sn^{IV} + L - H \rightleftharpoons Sn^{IV}LH_{-1}$	25.55 (0.27)	
$Sn^{IV} + L - 2H \rightleftharpoons Sn^{IV}LH_{-2}$	19.67 (0.045)	
$Sn^{IV} + L - 3H \rightleftharpoons Sn^{IV}LH_{-3}$	10.71 (0.10)	

* Hydrolysis constants for Sn(IV) were obtained from literature (38) and included in the model.

The charges were omitted for simplicity.

The formation constants obtained for the interaction of Sn(IV) with Cysteine were extracted by the ESTA program from the potentiometric data. These three stability constants, which are all hydroxyl species produced high standard deviations and Hamilton R-factor. The standard deviation for $Sn^{IV}LH_{-2}$ is reasonably low. This species will predominate in the pH range of 6-8 and

therefore despite the uncertainty of the model overall the situation at pH = 7.4 can still be described with some certainty. This is of course the aim of the study as the constants found with potentiometry are used in the blood plasma model for Sn(IV). These results are represented graphically in the $\bar{Q}$ curve (Figure 4.6) which is the average number of protons lost due to complexation. The calculated data represented by the solid lines do not match the experimental data (points) perfectly, especially at low pH. It is also evident that hydroxyl species are present because the $\bar{Q}$ curves lie above the $\bar{n}$ line. The graph is plotted from pH 4 to 12 because at low pH range, precipitation occurs and it is due to the unavoidable hydrolysis of Sn(IV). The points were omitted on that particular pH range because a precipitate forms which removes some of the compounds that are measured from the real solution. A disadvantage of the hydrolysis of Sn(IV) can sometimes arise in cases when a postulated complex species turns out to be an error absorbing parameter, there actually being no chemical justification for having postulated the species concerned. Such false species tend to appear when the experimental conditions have not been adequately controlled, therefore several attempts were tried in order to avoid the hydrolysis of Sn(IV).

Firstly the titrations were performed with solutions of Sn(IV)-Cysteine and titrating with NaOH but the results were not satisfactory as too much precipitation was experienced. Secondly, investigating reversible complexation whereby the titrations are started at high pH values was also unsuccessful in controlling the precipitation. It was thought that the ligand, deprotonated at high pH values, could interact with the metal-ion to counteract precipitation.

The last method was weighing Sn(IV) directly into the reaction vessel without dissolving it in HCl and obtaining the exact mass of the metal-ion. Precipitation however still occurred throughout the experiment. It was decided to use data from the first attempt (where the Sn(IV)-Cysteine solution is titrated with NaOH) since less precipitation occurred compared to the other two. The points where precipitation occurred were omitted. Five titrations of different ratios (1:1, 1:2,

1:1.5, 2:1 and 3:1) were performed. When trying to refine the data from all the titrations the data proved insensible. Three titrations of the ratios 1:2, 1:3, and 1:1.5 were refined together as best as possible to get a better fit.

Irregularities in the low pH values observed in the $\bar{Q}$ curve remained despite the removal of data where precipitation occurred. It was deduced that it could be due to fine precipitation (or colloids) which was not visible enough, and points were not deleted and hence high standard deviations were found. The high Hamilton R-factor can be due to the fewer data points used to fit the model.

At pH 4 the $\bar{Q}$ curve is at 3 and $\bar{n}$ = 2, denoting that in the presence of the metal ion, three protons are lost on complexation per metal ion. The complex which is forming in this particular pH is $M - 3H + LH_2 \rightleftharpoons MLH_{-1}$. It was expected that at low pH, during the coordination of the Sn(IV) with water, the formation of the MLOH species will occur because Sn(IV) has very high hydrolysis constants. This constant should be in the same order as the dissociation constant of metal-coordinated water molecules obtained in the literature. However this is not noticeable in the model because of the imprecise curves at the low pH values. Also looking at the $\log\beta_{11\text{-}3}$ = 10.71 it can be assumed that it corresponds to the dissociation constant of the ligand pK_1 (Table 4.1) which is equal to 10.28. This constant implies that the loss of a proton is due to the deprotonation at the amine site. This was to be expected in the high pH values because the ligand loses protons from the amine site when the solution becomes basic thus making binding interaction possible.

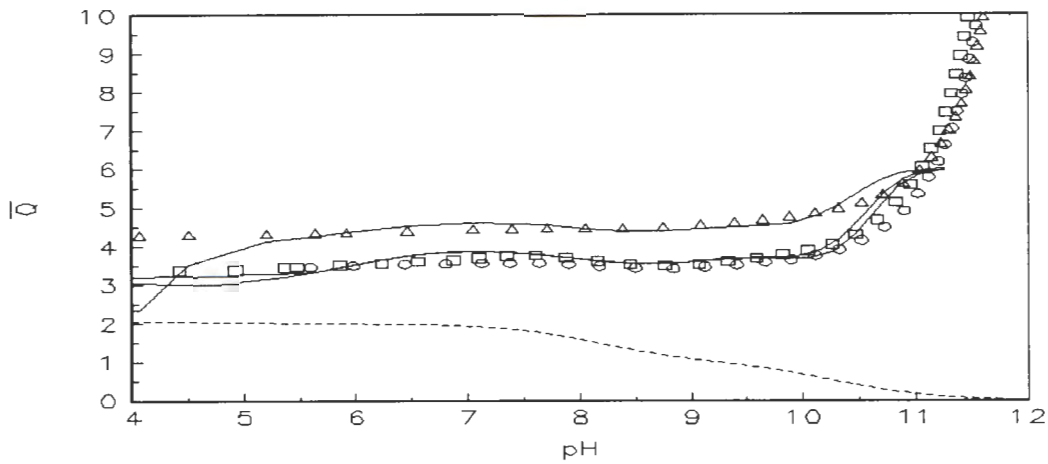

Figure 4.6 Experimental (points) and modeled (lines) deprotonation curves for Sn(IV)-Cysteine. *The dashed line is the $\bar{n}$ curve and represents the protonation state of the ligand in the absence of the metal-ion. The three titrations are represented by (O) 0.001378 M Cysteine, 0.0007026 M Sn(IV) and 0.015156 M HCl , (Δ) 0.002083 M Cysteine, 0.0007136 M Sn(IV) and 0.015806 M HCl and, (□) 0.000445 M Cysteine, 0.0006864 M Sn(IV) and 0.0141182 M HCl. All solutions were at 25°C and held at 0.15 M total ionic strength.*

Since we suspect that the hydrolysis of Sn(IV) makes the calculation of pL undefined the $\bar{Z}$ curves were of no use and are therefore not shown.

Subsequent to the performance of potentiometric studies of the interaction of Sn(IV) with Cysteine in aqueous solution, the proposed speciation distribution for the complexation can be seen in the figure 4.7.

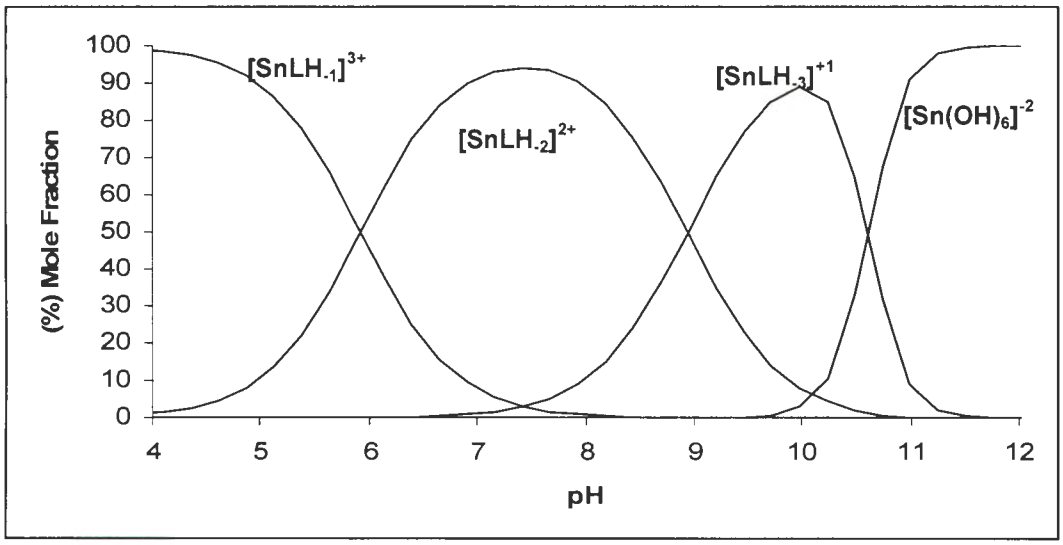

Figure 4.7 Speciation distribution curve for Sn(IV)-Cysteine at 25°C and in 0.15 M NaCl as calculated from formation constants in Table 4.2

When studying this graph it can be seen that it corresponds with the $\bar{Q}$ graph. All the complex species formed are hydroxy species in the pH range investigated. It can be assumed that the distortion observed in the $\bar{Q}$ graph at low pH values is the result of formation of $[SnL(OH)]^{3+}$. Therefore it can be deduced that the reason for the precipitate formation at this low pH is because the ligand is still fully protonated and it is not easy for the reaction between the metal and ligand to occur. Instead water reacts easier with the metal-ion resulting in the formation of the hydrolyzed species, and hence precipitation. This can be scheduled by calculating if free Sn^{4+} is exceeding the solubility product of $Sn(OH)_4$

At the physiological pH 7.4, there are three species present and the predominating one is $[SnLH_{-2}]^{2+}$ with 90% formation, where L is Cysteine and has no charge (neutral). The other two species which are $[SnLH_{-1}]^{3+}$ and $[SnLH_{-3}]^{1+}$ have the formation of 3% each. Figure 4.8 shows the species present in the physiological pH of interest. The standard deviation for constants for the $[SnLH_{-2}]^{2+}$ species formation was reasonable and therefore the situation in blood

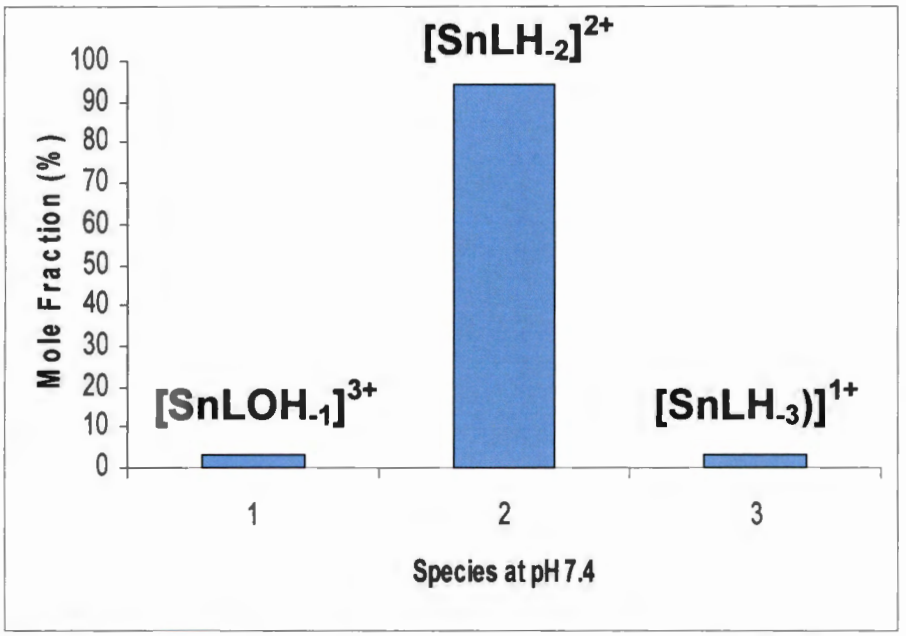

Figure 4.8 Speciation of Sn(IV)-Cysteine at pH 7.4

Since Cysteine contains a polar side chain which has the potential to form a further bond to the metal-ion, coordination with the sidechain depends on the nature of the metal-ion. According to the theory of hard and soft acid bases (HSAB), Sn(IV) prefers to bind to nitrogen donor and oxygen containing ligands rather than to ligands with sulfur donors hence the formation of this predominating species. Sn(IV) is regarded as a hard acid because it has high positive charge and small radius and it presents no unpaired electrons in the valence shells. Because Sn(IV) is a hard acid, it favours bonds to hard ligands such as water, therefore the complexation with aqua-ions is likely hence the hydrolysis. Figure 4.9 shows the complex structure that can be proposed for the predominating species at the pH of blood plasma.

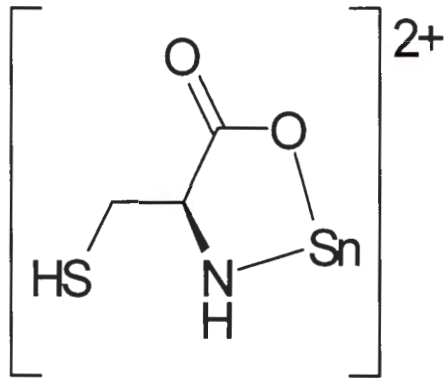

$[MLH_{-2}]^{2+}$

Figure 4.9 Possible structure for Sn(IV)-Cysteine at pH 7.4

4.2 Speciation for Histidine with Sn(IV)

4.2.1 Protonation constants

The protonation constants obtained in this study at 25°C at the ionic strength of 0.15 M NaCl are marginally higher than those found in the literature [12]. Good fits, indicated by low Hamilton R-factors and standard deviations in log K values, were obtained in these titrations.

Table 4.3: The Protonation constants for Histidine performed at ionic strength of 0.15M NaCl at 25°C.

Cation factor	Equilibrium species	log K	Literature[18]	Hamilton R-Factor
H^+	$H + L \rightleftharpoons LH$	9.11 (0.005)	8.99	0.00673
	$H + LH \rightleftharpoons LH_2$	6.09 (0.01)	6.03	
	$H + LH_2 \rightleftharpoons LH_3$	1.76 (0.01)	1.97	

The ring of Histidine is protonated in acidic solutions and de-protonated in basic solutions. This can be supported by looking at the structure of this ligand. Histidine is an imidazole-substituted alanine, an aromatic compound which is cyclic, planar and has three pairs of delocalised Π electrons. It has been observed that the ring of Histidine is protonated in acidic solutions and de-protonated in basic solutions because the pK_a of the protonated imidazole ring is 6.0, according to the literature [6]. The reason for this ligand to remain protonated at low pH is because of the non-bonding electrons which are readily available to accept the proton when introduced into the solution. But surprisingly, not all nitrogen atoms in the compound gain the proton. Within the structure the doubly bonded heterocyclic nitrogen (imidazole) will accept protons and this is due to the resonance resulting from nitrogen's lone pair with the benzene ring.

This occurs through p-orbital overlap. The resonance not only decreases the availability of the nitrogen's lone pair but also adds stability to aromatic amines, making them less reactive.

The degree to which the protons dissociate from Histidine is according to the pK_a's of carboxyl and amino groups and the pH of the solution. The pK_a of α-COOH is 1.82 and α-NH_3^+ is 9.17 [6]. The protonated imidazole side chain of Histidine has a pK_a of 6.04, therefore it will lose a proton before the amino group. On the ring the pyrrole N cannot lose a proton even if an excess base is added because its pK_a value is about 14.

Histidine can exist in four different forms and the form that predominates depends on the pH of the solution.

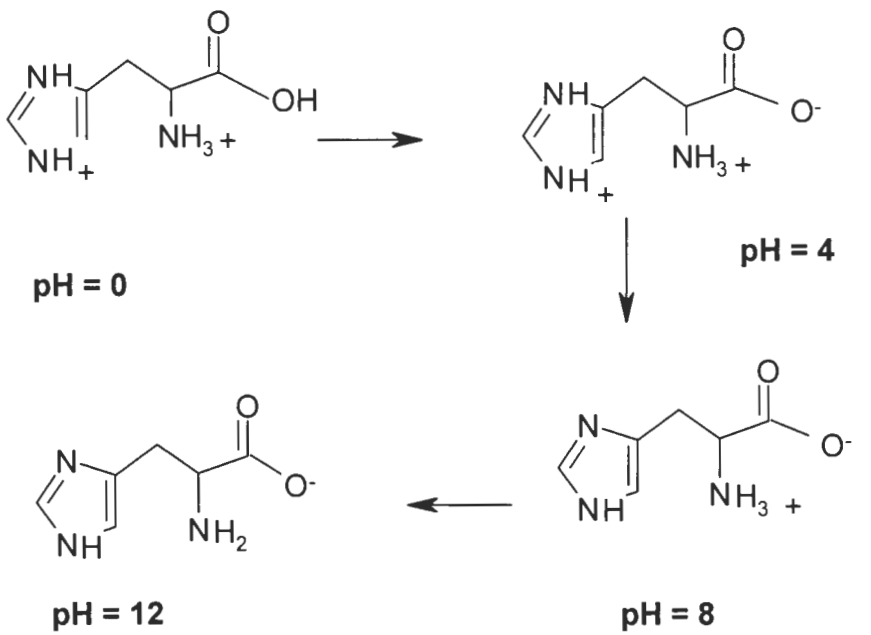

Figure 4.10 Proposed protonation schemes for Histidine

The average number of protons bound per Histidine is represented in the graph in Figure 4.11. The graphical representation of the model shows good concurrence between the calculated curve and the experimental data.

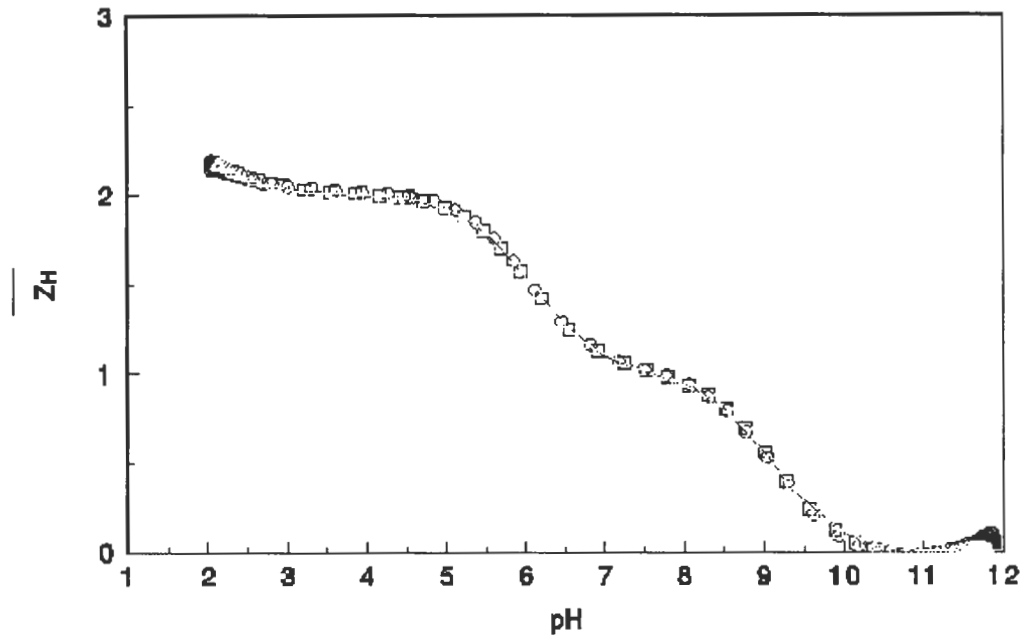

Figure 4.11 Protonation curve studied for Histidine

Experimental (points) and modeled (lines) proton formation curves for Histidine. The three separate titration are represented by (O) 0.0012 M Histidine and 0.0125 M HCl, (Δ) 0.0018 M Histidine and 0.0135 M HCl, (□) 0.0025 M Histidine and 0.0125 M HCl. All solutions were at 25^{0}C and 0.15 M NaCl.

The protonation curve and the dissociation constants obtained reveal that Histidine exhibits three protonation sites. At pH 2.8 one proton is lost from the carboxylic group which has a lower pK_a than protonated amines. The other two remaining protonation constants (pK_2 and pK_3) shows that dissociations are due to the amine sites.

The pK_2 = (6.0934) is due to dissociation at the imidazole N, because it has a much lower pK_a and hence is mainly deprotonated at physiological pH. On the ring the pyrrole N cannot loose a proton even if an excess base is added.

The species distribution curves for the protonation of Histidine as shown below in Figure 4.12 were plotted for the titrations of the pH range shown on the graph.

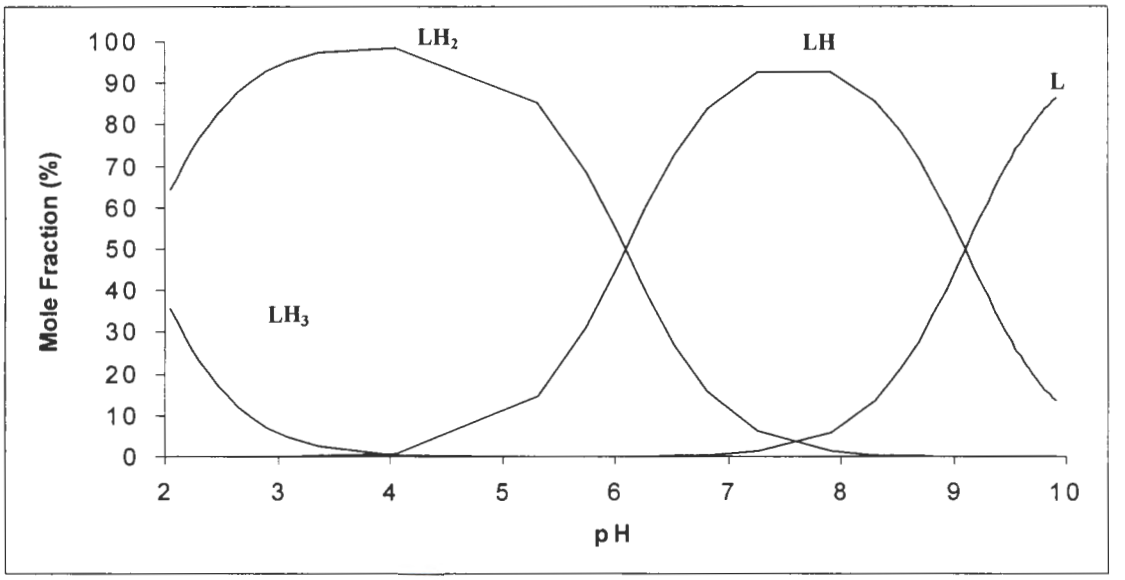

Figure 4.12 Species distribution curve for the protonation of Histidine at 25°C and 0.15 M NaCl as calculated from the proto nstants in Table 7.

The distribution of the individual species co-existing in equilibrium in this system corresponds well with the protonation equilibria in Figure 4.11.

At a pH of 2 the LH_3 species constitutes 35 % of the ligand. This is the pH range where the LH_3 species dominates and starts to dissociate. At the pH of blood plasma and of interest for *in vivo* studies, there is an existence of 8 % of LH_2 with the formation of the dominating specie LH (90 %). At pH > 10 the remaining species is the free ligand.

4.2.2 Complexation of Histidine with Sn(IV)

4.2.2.1 Metal-ligand formation constants for Sn(IV)-Histidine

The experiments were performed at 25°C ± 0.1 and ionic strength of 0.15 M NaCl. The pK_w was fixed at 13.79 for these conditions. Hydrolysis constants for Sn(IV) were included in the model. Five titrations of different ratios were performed but they were not all used. When trying to refine the data from all the titrations the data proved to be insensible. Therefore only three titrations of the ratios 1:1, 2:1 and 1:1.5 (L:M) were refined together as best as possible to get a better fit. The points where precipitation was observed were excluded from the model. The data in those particular ratios, 3:1, 1:2(L:M) did not refine because of precipitation. In calculating the stability constants, hydroxy species were taken into consideration since the metal-ion, Sn(IV), reacts readily with water. Table 4.4 contains the log β values determined for the complexation of Sn(IV) with Histidine.

Table 4.4: The overall stability constants for Histidine with Sn(IV) obtained in this work

Equilibrium species #	log β	Hamilton R-Factor
$Sn^{IV} + OH \rightleftharpoons Sn^{IV}OH$	-1.94*	
$Sn^{IV} + 6\ OH \rightleftharpoons Sn^{IV}(OH)_6$	-24.11*	
$Sn^{IV} + L - H \rightleftharpoons Sn^{IV}LH_{-1}$	26.82 (0.52)	0.11029
$Sn^{IV} + L - 2H \rightleftharpoons Sn^{IV}LH_{-2}$	18.98 (0.18)	
$Sn^{IV} + L - 3H \rightleftharpoons Sn^{IV}LH_{-3}$	10.20 (0.20)	

Charges on the species ignored for the sake of simplicity

* Hydrolysis constants obtained from literature [38]

The stabilities of the different types of species that forms in complexation equilibria depend upon the experimental conditions used. The complexation equilibria of this system have shown the presence of the following species, MLH_{-1}, MLH_{-2} and MLH_{-3}. By looking at the measure of difference between the parameters that were refined and the experimental data, it can be clearly deduced that there was an experimental error. In an effort to make the uncertainties and the Hamilton R-factor lower was to fix the first constant and refine the other constants as there were correlations between the complexes. The standard deviations of the two complexes were slightly reduced although the Hamilton R-factor remained the same. To test the validity of the model chosen the $\bar{Q}$ graph (the average number of protons released on complexation per metal-ion) was plotted in Figure 4.13

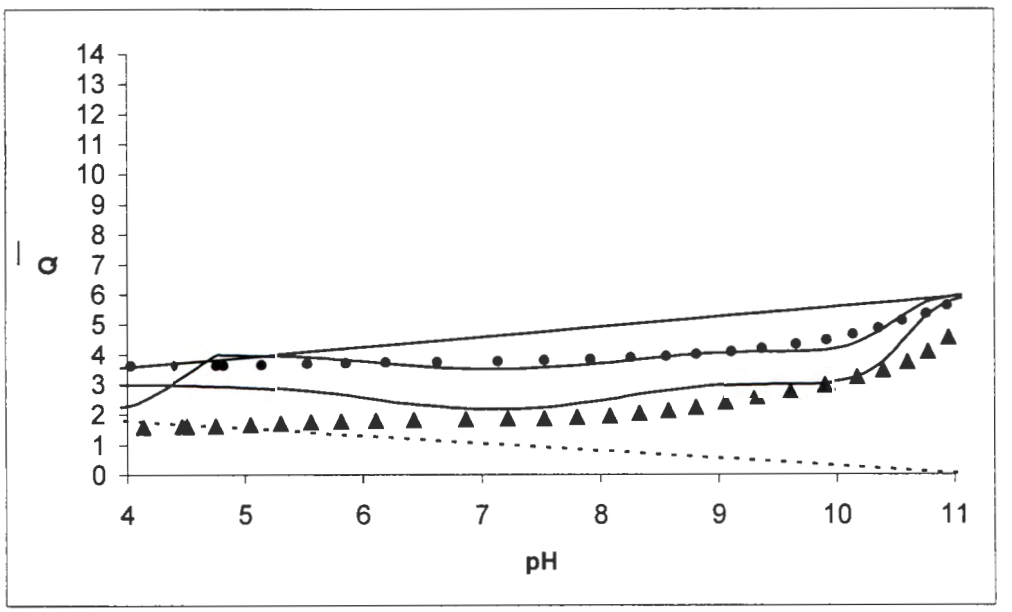

Figure 4.13 Experimental (points) and modeled (lines) deprotonation curves for Sn(IV)-Histidine. *The dashed line is the $\bar{n}$ curve and represents the protonation state of the ligand in the absence of the metal-ion. The three titrations are represented by (O)0.0007476 M Histidine, 0.0006879 M Sn(IV) and 0.0136731 M HCl (Δ)0.0013838 M Histidine, 0.0006901 M Sn(IV) and 0.0137778 M HCl and, (□)0.000446 M Histidine, 0.0006854 M Sn(IV) and 0.013673 M HCl All solutions were at 25°C and held at 0.15 M total ionic strength.*

The calculated data (solid line) are not in good agreement with the experimental data (points) for all three titrations and this does not lend credibility to the chosen model. The deprotonation curve also casts doubt on the validity of the model. No suitable models were achieved especially for the third titration. The data in this titration were very difficult to model. Removing data of this titration from pH 4 to 11 did not improve the fit.

When examining the graph of average number of protons lost by the ligands due to complexation at certain pH values, the $\bar{Q}$ line lies above the $\bar{n}$ line (average number of protons bound per ligand in the absence of complexation) in the set pH range and this provides evidence that the hydroxyl species are present.

The graph was plotted from pH 4-11 because the points were omitted where precipitation was observed. The omission was done because the reaction of water with Sn(IV) complicates the study of chemical equilibrium in this case, though it proved to be fruitless because the irregularities in the graph were still experienced in the low pH values. Therefore the $\bar{Q}$ graph in figure 4.13 shows that the fit is inefficient and these values are only an indication and cannot be used in the blood plasma model.

According to the way Histidine dissociates, the coordination of Histidine to the metal-ion, Sn(IV) is not expected at the beginning of the titrations because Histidine is protonated at this pH value. It is assumed that the coordination of Sn(IV) with Histidine is possible from pH 4 which will result in the loss of a proton from the ligand. The point where it coordinates in the ring should be consistent with tridentate coordination indicating that the proton is released from the carboxyl group and not coordinated water molecule. This is not evident from the model. Observing the formation constant obtained log $K_{11\text{-}3}$, it is not of similar magnitude to the $pKa_1 = 9.11$ (protonation constant in Table 4.3) and also it is not close enough to the first hydrolysis constant to assume that the deprotonation is from a metal-coordinated water molecule.

Since this model does not produce satisfactory fit to the titration data points, the $\bar{Z}$ curves could not be plotted. The species distribution curves for the chosen model are displayed in figure 4.14.. From this curves various complexes can be seen at the pH values predicted by the deprotonation curves.

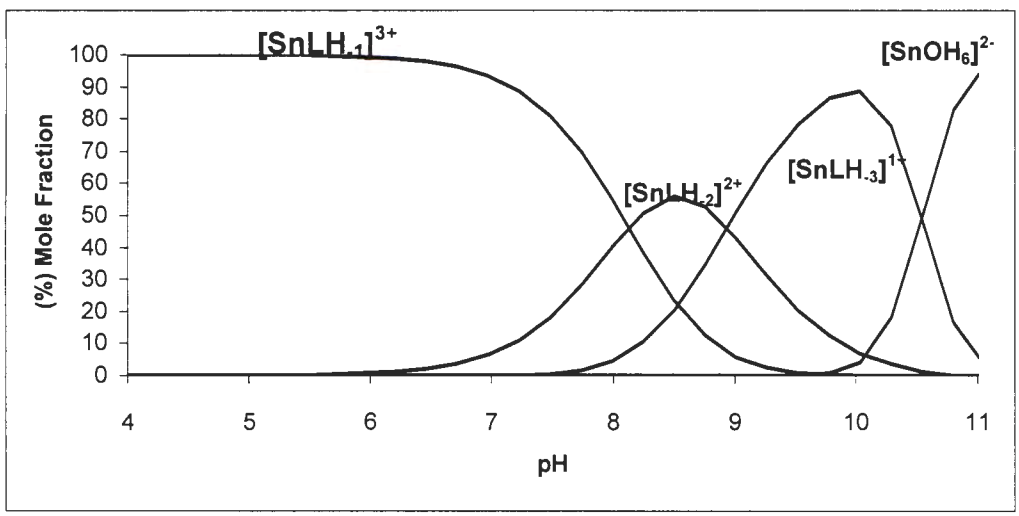

Figure 4.14 The species distribution curve shows the relative distribution of the complexes forming.

This diagram shows that the complexes that are formed are indeed all hydroxyl species as seen in the $\bar{Q}$ graph. The species that forms at low pH is $[MLH_{-1}]^{3+}$. At physiological pH 7.4, the species that forms is the MLH_{-1} species, which constitutes 80%. It can be postulated that it this compound that is responsible for the precipitation that forms in this pH range therefore resulting in the high standard deviations and the problematic fit observed in the $\bar{Q}$ graph. In the high pH values in the $\bar{Q}$ there are also irregularities, and looking at the species distribution curve there is formation of the hydrolyzed species, $[ML(OH)_6]^{2-}$. It was found that water interacts strongly with Sn(IV), especially at basic pH. The problematic fit observed in the deprotonation curve at high pH are the result of the hydrolysis; $[Sn(OH)_6]^{2-}$. The hydrolyzed species form fine precipitates that are not well handled by these methods as described earlier.

The speciation for the Sn(IV) with Histidine at physiological pH can be seen in Figure 4.15

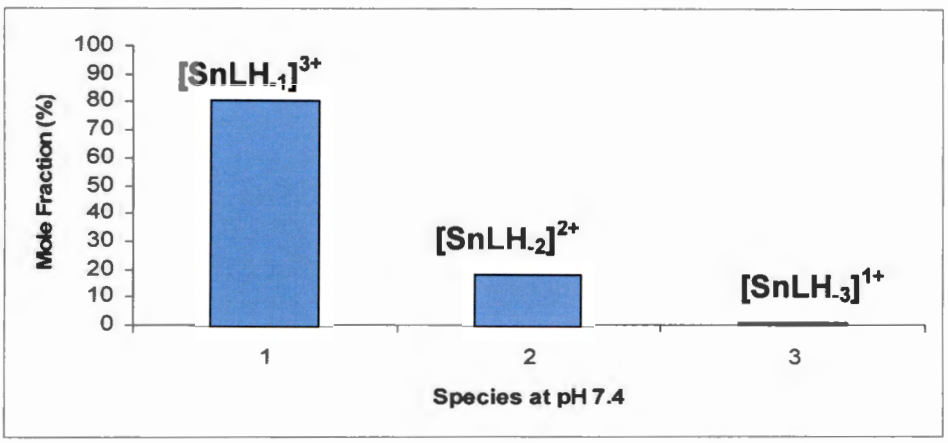

Figure 4.15 Speciation for Sn(IV)-Histidine complexes at pH 7.4

At pH 7.4 there are three species forming $[MLH_{-2}]^{2+}$ (19%), $[MLH_{-3}]^{1+}$ (1%) with the predominating species being $[MLH_{-1}]^{3+}$ (80%) where L is Histidine. Unfortunately not even the formation constant for this species is well defined and therefore the complexation at blood plasma pH can not be accurately determined. Due to the hydrolysis that seems to predominate throughout, one suspects that Sn(IV) forms very weak complexes with Histidine and therefore will not influence the speciation of Sn(IV) in blood plasma. The formal charge of the ligand is neutral. It can be deduced that this complex forms because the molecule is zwitterionic at this pH, that is, it can act as both an acid and a base. Binding is unlikely at this pH and therefore Sn(IV) can only weakly bind to the oxygen on the ligand because the positive charge on the NH_2 site (at this pH) causes repulsion of the metal ion. This weak complexation means that the hydrolysis species predominate resulting in the precipitate. The suspecting predominating complex at physiological pH is shown in Figure 4.16.

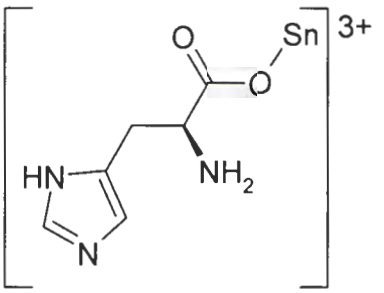

Figure 4.16 Proposed structure of the predominant species at pH 7.4

4.3 Remodelling of both systems, (Sn(IV)-Cysteine and Sn(IV)-Histidine

As there were difficulties encountered in finding the best model to describe the experimental data of both systems, a decision was taken to include other Sn(IV) hydrolysis constants as they could affect complexation of this metal ion with the respective ligands. In an attempt to improve on the model of both systems, hydrolysis data were estimated using an acidic metal ion similar to Sn(IV) namely Pa(IV) reported in Martell [40]. Pa(IV) was used because is the only tetravalent metal ion with many hydrolysis constants reported in the literatur. Each system was modeled separately to obtain a new model. This was modeled with the titration data of L:M, 2:1 and 3:1 and complexes 11-1, 11-2 and 11-3 with the following different Sn(IV)-OH constants included (Table 4.5) and each model refined as best as possible.

Table 4.5: Hydrolysis constants for Sn(IV)

Equilibrium species #	log β Pa(IV)	log β Sn(IV)	Conversion for ESTA input
Sn^{IV} + OH	14.4	11.8	$Sn^{IV}(OH)_1$ = -1.94
Sn^{IV} + 2OH	13.8	25.3	$Sn^{IV}(OH)_2$ = -2.28
Sn^{IV} + 3OH	12.9	38.2	$Sn^{IV}(OH)_3$= -3.17
Sn^{IV} + 4OH	10.7	48.9	$Sn^{IV}(OH)_4$= -6.3

Although both systems were remodeled they showed the same results and proved to be unsuccessful. Species remain inaccurate and practically unresolved within this experiment as the standard deviation were still high. The first constant was fixed and other constants refined as there were correlations between the complexes. Acid concentration decreased by 16% before converging which is not acceptable. When changing the acid concentration it was found that the 11-2 complex is rejected and that the log constants of 11-1 and 11-3 which were originally 24 and 10 increased to 45 and 23 respectively.

The results of remodeling both systems Sn(IV)-Cysteine and Sn(IV)-Histidine using hydrolysis constants calculated how Pa(IV) are represented in the $\bar{Q}$ graphs. These curves are shown in figures 4.17 and 4.18.

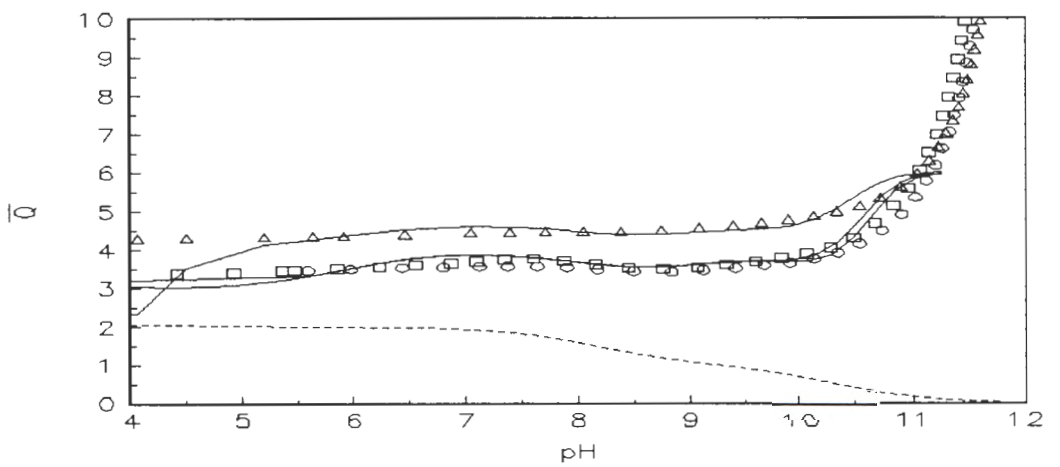

***Figure* 4.17 Deprotonation curves for Sn(IV)-Cysteine using the hydrolysis constants deduced from Pa(IV)**

Experimental (points) and modeled (lines) deprotonation curves for Sn(IV)-Cysteine. The dashed line is the $\bar{n}$ curve and represents the protonation state of the ligand in the absence of the metal-ion. The three titrations are represented by (O) 0.001378 M Cysteine, 0.0007026 M Sn(IV) and 0.015156 M HCl , (Δ) 0.002083 M Cysteine, 0.0007136 M Sn(IV) and 0.015806 M HCl and, (□) 0.000445 M Cysteine, 0.0006864 M

Sn(IV) and 0.0141182 M HCl. All solutions were at 25°C and held at 0.15 M total ionic strength.

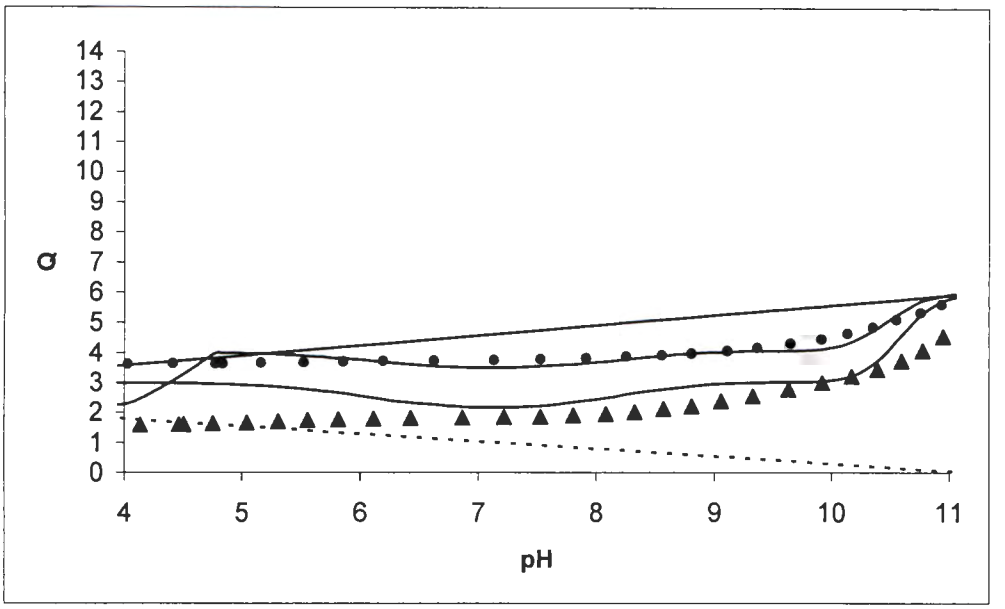

***Figure* 4.18 Deprotonation curve for Sn(IV)-Histidine using the hydrolysis constants deduced from Pa(IV)**

Experimental (points) and modeled (lines) deprotonation curves for Sn(IV)-Histidine. The dashed line is the $\bar{n}$ curve and represents the protonation state of the ligand in the absence of the metal-ion. The three titrations are represented by (O)0.0007476 M Histidine, 0.0006879 M Sn(IV) and 0.0136731 M HCl (Δ)0.0013838 M Histidine, 0.0006901 M Sn(IV) and 0.0137778 M HCl and, (□)0.000446 M Histidine, 0.0006864 M Sn(IV) and 0.013673 M HCl. All solutions were at 25°C and held at 0.15 M total ionic strength.

The two models presented above were the most sensible that could be derived and refined. The complexation equilibria have shown the presence of the following species, MLH_{-1}, MLH_{-2} and MLH_{-3} in the systems. Irregularities observed in the $\bar{Q}$ curves remained despite the addition of estimated hydrolysis constants. The $\bar{Q}$ for these models predominantly lie above the $\bar{n}$ for the entire pH range, which is indicative of more free protons from the system being detected by the glass electrode than expected. This could be due to the hydrolysis of the Sn(IV) which is typically unavoidable in water rendering the

ESTA analysis results rather distorted. The experimental curves deviate from the calculated curves for both systems and this does not lend credibility to the chosen model. The deprotonation curves cast doubt on the validity of the models.

Determination of solubility product, K_{sp}

In modeling the speciation of Sn(IV) it has been necessary to evaluate all possible metal-ligand interactions since the precipitation of tin complexes in the titration vessel during a potentiometric titration was a relatively common phenomenon. It was assumed that there are possibilities that precipitate observed could be due to $Sn(OH)_4$. The first appearance of a precipitate in the vessel indicates that saturation has been reached and the solubility product, K_{sp} has been exceeded.

Pu(IV) was the only reported metal hydroxide in Martell that could be used as estimated value for Sn(IV) since there is no reported K_{sp} value for $Sn(OH)_4$. $Pu(OH)_4$ has a K_{sp} value of 5×10^{-48}.

The solubility product (K_{sp}) at different pH's and free Sn concentrations were determined from the experimental values obtained from ESTA species distribution modeling. This solubility product can be expressed in the general equilibrium as $M_pL_q(s) \leftrightarrow pM + qL;\ K_{sp} = [M]^p[L]^q$

Therefore $Sn(OH)_4 \rightleftharpoons Sn^{4+} + 4OH^-\ ; K_{sp} = [Sn^{4+}]\,[OH^-]^4$

The $[OH]$ was calculated from the experimental pH values using $pk_w = pH + pOH$ or $-\log K_w = -\log[H^+] - \log[OH^-]$

The calculated K_{sp} values were compared with the $K_{sp}\,(Pu(OH)_4) = 5\times10^{-48}$ which is approximated by K_{sp} for $(Sn(OH)_4)$.

The solubility product of a soluble salt can be calculated if the concentrations of free metal and ligand just before precipitation are known. Thus, aqueous free

ligand and free metal ion concentrations can be calculated at the point of precipitation if the ligand protonation and metal-ligand formation constants are known in addition to the free hydrogen ion concentration [38].

This perceived problem was further investigated by checking the ESTA values for free Sn(IV) to verify if the solubility product of $Sn(OH)_4$ is not exceeded. While the calculated K_{sp} values are smaller than the estimated K_{sp} of 5×10^{-48} no precipitation should form.

Solubility products calculated from the precipitation points are given in Table 4.6.

Table 4.6 Determination of the solubility product (K_{sp}) of $Sn(OH)_4$ at 25°C , I = 0.15 M NaCl

pH	[OH]	Free [Sn^{IV}]	K_{sp}
1.865	1.19×10^{-12}	9.829×10^{-19}	1.971×10^{-66}
2.456	4.63×10^{-12}	1.029×10^{-20}	4.747×10^{-66}
3.972	1.52×10^{-10}	2.659×10^{-28}	1.42×10^{-66}
5.177	2.44×10^{-9}	7.173×10^{-29}	2.53×10^{-64}
7.284	3.12×10^{-7}	4.405×10^{-39}	4.168×10^{-60}
9.993	0.0002	1.87×10^{-41}	1.21×10^{-56}
11.197	0.0026	4.204×10^{-45}	1.78×10^{-55}

The results in table 4.6 showed that the K_{sp}'s are in the order of magnitude 7 smaller than the estimated K_{sp} and thus even if the K_{sp} was incorrectly estimated the conclusion that precipitation do not form over the pH 1.8 to 11.2 range will still be true. It seems there is no problem with the free ligand concentrations because the solubility is always lower than the estimated K_{sp} in this experiment.

CHAPTER 5

CONCLUSION

5.1 CONCLUSION

The main aim of this study was to determine the possible complexes that can form when Sn(IV) interacts with the selected blood plasma ligands, Cysteine and Histidine. The knowledge of the binding interaction between these Sn(IV)-ligand complexes will be used in the attempt to establish an Sn(IV) blood plasma model which will be used to determine the biodistribution of potential Sn(IV)complexes in blood plasma with the speciation model ECCLES. The estimation of the protonation constants for the two ligands, Histidine and Cysteine were obtained and they were comparable to the data found in the literature. Protonation of these two ligands on carboxyl and amino groups shows that dissociation of the amino acid in solution is pH dependent.

All the complexes that were formed by the two ligands with Sn(IV) are the hydroxyl species and this is due to the hydrolyzed metal-ion. Reaction of water with Sn(IV) complicates the study of chemical equilibrium in solution. The presence of solvent crowd around the species formed during a chemical reaction affects the thermodynamic parameters for the equilibrium attainment. The high Hamilton R-factor and standard deviation cast a doubt to the results obtained. This could also be illustrated with $\overline{Q}$ graphs where the fit of the theoretical curve and the experimental data was not good. With complexation of Cysteine and Sn(IV), this ligand is a real ambidentate therefore the coordination chemistry of the compound is rather complicated and depend largely on the nature of the metal-ion. Since Sn(IV) is a hard metal it prefers to coordinate to oxygen and amine donors. The predominating complex that exists for the complexation of Sn(IV) with Cysteine in pH 7.4 is $[MLH_{-3}]^{2+}$ with 90% formation. The standard deviation for this complex was relatively low which gives confidence that the situation at pH=7.4 can be described.

However for the Sn(IV)-Histidine complexes not one of the standard deviations were low. It is therefore not advisable that the constants determined here be included in the blood plasma model. If the determined formation constants are used the speciation of Sn(IV)-Histidine at physiological pH shows the formation of a high percentage (80%) of $[MLH_{-1}]^{3+}$.

The main problem in attaining more plausible models was the formation of Sn(IV) hydroxide species through hydrolysis. This implies that the complexes that Cysteine and Histidine form with Sn(IV) are not very strong and therefore will not compete significantly for Sn(IV) if a stronger complex would be introduced in a medium for instance blood plasma. Also the other hydrolysis constants of Sn(IV) were estimated from the similar metal ion Pa(IV) and included in the model, but the model still proved to be insensible. The results showed that remodeling seemed fruitless in lowering uncertainties of the individual species. The solubility product of $Sn(OH)_4$ were calculated and it seems there is no problem with the free ligand concentrations because the solubility is always lower than the estimated K_{sp} in this experiment.

As very few constants for Sn(IV) have been measured or exist in the literature no blood plasma modelling was undertaken in this study.

5.2 RECOMMENDATIONS AND FUTURE WORK

Since hydrolysis of Sn(IV) was the major obstacle experienced in the experiments, more attention should be focused on developing a method of standardizing tin solutions in order to get the exact concentration of this metal-ion when using it. The other alternative that can also be tried is to weigh the tin salt directly into the vessel without dissolving it to get its exact mass to avoid standardizing it. This hydrolysis, which leads to precipitation, makes the results rather unclear. The complexation system results obtained are not reliable, as the precipitation formed during titrations. It is also possible that precipitation formed

at higher pH values, which was not visible to the human eye and lead to a distortion in the results. If the concentration of the metal can be lowered and a technique such as polarography used to study the metal ion concentration it also presents an option to avoid this hydrolysis as the ligands will be able to complexate small amounts of Sn(IV) more readily.

REFERENCES

References

1. Microsoft Encarta Premium Suite, 2004, 1993-2003 Microsoft Corporation.
2. O.L.M. Biljvoet, H.A. Fleisch, R.E. Canfield and G.A Rodan, Bisphosphonates on Bones Elsevier, Amsterdam, 1995, 358
3. Buck A. Rhodes, Quality Control in Nuclear Medicine, Radiopharmaceuticals, Instrumentation, and in vitro assays, 1977, 246-257
4. Harold L. Atkins et al, Radiology, 1993, 186, 179-283
5. David R. Jansen, The study of complexation of Sn(II)-APDDMP and Sn(IV)-PEI-MP considered as potential therapeutic agents for bone metastases, 2005
6. John McMurry, Fundamentals of Organic Chemistry, 1998, 4th edition, 474-491
7. Anderson K.K and Graslund A, Advanced Inorganic Chemistry 40.121, Mekee V 1993, Advanced Inorganic Chemistry 41, 323.
8. Marnix G.E.H. Lam, John M.H. de Klerk, Peter P. van Rijk, European J. Nuclear Medicine and Molecular Imaging,, 2000
9. Techniques in Regional Anesthesia and Pain Management, 9 Issue 3, July 2005,177-183
10. A.J.B. McEwan, Seminars in Radiation Oncology, 2000, **10**, 103-114
11. W.A. Volkert, J. Nucl. Med, 1991, 32, 174
12. W.K.A. Louw, I.C. Dormehl, A.J. van Rensburg, N. Hugo, A.S. Alberts, O.E. Forsyth, G. Beverley, M.A. Sweetlove, J. Marais, M.G. Lotter, A.van Aswegen, Nucl. Med Biol, 23, 1996, 935-941

13. N.V. Jarvis, J.M. Wagener, G.E. Jackson, J. Chem. Soc. Dalton Trans.,1995, 1411-1415

14. J.M. Wagener and N.V. Jarvis. S. Afr. J. Chem., 1995, **48**, 85-90

15. J.A. Bevan, A.J. Tofe, J.J. Benedict, M.D. Francis and B.L. Barnett, J. Nucl. Med., 1991, 32, 174-185

16. E. Savio et al, BMC Nuclear Medicine, 2001, 1, 2-17

17. J.C.P. Heggie, J. Nucl. Med., 1991, 5(32), 840-844

18. J.R Zeevaart, PhD thesis, Metal-ion Speciation in Blood Plasma as a Tool in Predicting the *in vivo* Behaviour of Potential Bone-Seeking Radiopharmaceuticals, 2001

19. J.R Zeevaart, N.V. Jarvis, I. Cukrowski and G.E. Jackson, S. Afr. J. Chem.,1997, 50(4), 189-194

20. J.R. Zeevaart, N.V. Jarvis, W.K.A. Louw, G.E. Jackson, Journal of Inorganic Biochemistry, 1999, 73, 265-272

21. J.R. Zeevaart, N.V. Jarvis, W.K.A. Louw, G.E. Jackson, Journal of Inorganic Biochemistry, 2001, 83, 57-65

22. R.A.M.J. Claessens and Z.I. Kolar, Langmuir, 2000, 16, 1360-1367

23. J.R. Zeevaart, David R. Jansen, M, Filomena Botelho, Antero Abrunhosa, Celia Gomes, Luiz Metello, Zvonimir I.Kolar, Gerard C. Krijger, Werner K.A. Louw, Irene C. Dormehl, Journal of Inorganic Biochemistry, 98, 2004, 1521-1530

24. I.C. Dormehl, W.K.A. Louw, R.J. Milner, E. Kilian, and F.A.H. Schneewesis, Drug Res, 2001, 54, 258-263

25. J.R. Zeevaart, W.K.A. Louw, Z.I. Kolar, J.M. Wagener, N.V.Jarvis, R.A.M. Claessens, Journal of Radioanalytical and Nuclear Chemistry, 2003, 257, 83-91
26. D.A. Skoog, D.M. West, F.J. Holler, Fundamentals of Analytical Chemistry, 4th Edition, 1982, 317
27. F. Albert Cotton and Geoffrey Wilkinson, Advanced Inorganic Chemistry, 4th edition, 1980 January.
28. Daniel Harris, Quantitative Chemical Analysis, 1998, 375
29. Perrin and Agarwal, Computer-based approach to chelation therapy a theoretical study of some chelating agents for the selective removal of toxic metal ion from plasma, 1976, September 6(5), 667-73
30. Guy Berthon, HandBook of Metal-Ligand Interactions in Biological Fluids, Bioinorganic Chemistry Volume 1, 1995, 524-530
31. F.R. Hartley, C. Burgess, R. Alcock, Solution Equilibria, John Wiley and Sons, 1980
32. Peter Letkeman, Journal of Chemical Education, 1996, 73, 165
33. http:// www.chemical /speciation. Html.
34. Peter William Linder, Department of Chemistry, University of Cape Town, Rondebosch
35. Peter M. May, Kevin Murray, and David Williams, Talanta, 1985, 32, 483-489
36. Peter M. May, Kevin Murray, and David Williams, Talanta, 1988, 35, 825-830
37. P.M. May, D.R. Williams and P.W. Linder, J. Chem. Soc. Dalton Trans., 1977, 588.

38. J.R. Duffield, D.R. Williams, and I Kron, Polyhedron, 1991, 10, 377-387

39. Phillip S. Bailey J R, and Christina A Bailey, Organic Chemistry: a brief survey of concepts and application, 4th edition, 1989, 431

40. Smith Martell, Critical Stability Constants, Volume 4: Inorganic Complexes, 1976, 4

APPENDICES

Data for Sn(IV) – Cysteine

```
*******   ******  *******   *****
*       *         *    *    *
*       *         *    *    *
******    *****     *    *******
*           *    *    *    *
*           *    *    *    *
*******   ******     *    *    *

PROGRAM ESTA2A          VERSION 3.0



TASK OBJE  1       CYS1-SN+4
MODL      SN+4 CYS1 H +1
CPLX 0  1 -13.7900  SN+4( 0) CYS1( 0) H +1(-1)
CPLX 0  1  10.2803  CYS1( 1) H +1( 1)
CPLX 0  1  18.4262  CYS1( 1) H +1( 2)
CPLX 0  1  19.8815  CYS1( 1) H +1( 3)
CPLX 0  1  -1.9370  SN+4( 1) H +1(-1)
CPLX 0  1 -24.1080  SN+4( 1) H +1(-6)
CPLX 0  1  25.5839  SN+4( 1) CYS1( 1) H +1(-1)
CPLX 1  1  19.6696  SN+4( 1) CYS1( 1) H +1(-2)
CPLX 1  1  10.7079  SN+4( 1) CYS1( 1) H +1(-3)
CONC
VESL IVOL     24.847  0 0
VESL CYS1   .0013786  2 0
VESL H +1   .0150049  0 0
VESL SN+4   .0006956  0 0
BUR1 H +1  -.0504680  0 0
ELEC
ZERO H +1    401.023    0
GRAD H +1     59.154    0
WGHT 1
VESL CYS1   .0000028
VESL H +1   .0000303
VESL SN+4   .0000014
BUR1 H +1  -.0001009
ZERO H +1       .820
GRAD H +1       .120
TITR RNDE      .0010
EOBS RNDE      .0800
DATA

CONC
```

```
VESL IVOL     24.848  0 0
VESL CYS1   .0020838  2 0
VESL H +1   .0157023  0 0
VESL SN+4   .0007065  0 0
BUR1 H +1  -.0504680  0 0
ELEC
ZERO H +1    400.444    0
GRAD H +1     59.253    0
WGHT 1
VESL CYS1   .0000042
VESL H +1   .0000317
VESL SN+4   .0000014
BUR1 H +1  -.0001009
ZERO H +1       .820
GRAD H +1       .120
TITR RNDE      .0010
EOBS RNDE      .0800
DATA

CONC
VESL IVOL     25.037  0 0
VESL CYS1   .0004450  2 0
VESL H +1   .0139770  0 0
VESL SN+4   .0006795  0 0
BUR1 H +1  -.0504680  0 0
ELEC
ZERO H +1    403.079    0
GRAD H +1     59.131    0
WGHT 1
VESL CYS1   .0000009
VESL H +1   .0000282
VESL SN+4   .0000014
BUR1 H +1  -.0000100
ZERO H +1       .820
GRAD H +1       .120
TITR RNDE      .0010
EOBS RNDE      .0800
DATA


OPTIMIZATION CYCLE  0
**********
OVERALL OBJE OBJECTIVE FUNCTION:    3.5233E+02       (N-R
ITERATIONS:   493)
FORMATION CONSTANTS:
----------
```

```
COMPLEX NUMBER:       8         9
 LOG BETA:       19.6696    10.7079

GAUSS-NEWTON:              INITIAL SLOPE =  -5.1202E-06

                    SLOPE AT PREDICTED SOLUTION  =   -1.1119E-07


OPTIMIZATION CYCLE  1
*********************
OVERALL OBJE OBJECTIVE FUNCTION:     3.5233E+02       (N-R
ITERATIONS:  1067)
FORMATION CONSTANTS:
--------------------
COMPLEX NUMBER:       8         9
 LOG BETA:       19.6695    10.7078
 STD DEVN:         .0449      .1003

GAUSS-NEWTON:              INITIAL SLOPE =  -6.3263E-09


OPTIMIZATION CYCLE  2    (CONVERGENCE)
*********************
OVERALL OBJE OBJECTIVE FUNCTION:     3.5233E+02       (N-R
ITERATIONS:  1651)
FORMATION CONSTANTS:
--------------------
COMPLEX NUMBER:       8         9
 LOG BETA:       19.6695    10.7078
 STD DEVN:         .0449      .1003
NO SIGNIFICANTLY CORRELATED PARAMETERS FOUND
HAMILTON R-FACTOR:   .06324
HAMILTON  R-LIMIT:   .00339
NO. OF TITRATIONS:    3          NO. OF POINTS:  191
Stop - Program terminated.
```

Data for Sn(IV)-Histidine

```
*******   ******  *******   *****
*       *         *    *   *
*       *         *    *   *
******    *****     *    *******
*           *    *    *   *
*           *    *    *   *
*******  ******     *    *   *
```

PROGRAM ESTA2A VERSION 3.0

```
TASK OBJE  1       HIS1-SN+4
MODL     SN+4 HIS1 H +1
CPLX 0  1 -13.7900  SN+4( 0) HIS1( 0) H +1(-1)
CPLX 0  1   9.1086  HIS1( 1) H +1( 1)
CPLX 0  1  15.2020  HIS1( 1) H +1( 2)
CPLX 0  1  16.9630  HIS1( 1) H +1( 3)
CPLX 0  1  -1.9370  SN+4( 1) H +1(-1)
CPLX 0  1 -24.1080  SN+4( 1) H +1(-6)
CPLX 1  1  27.8638  SN+4( 1) HIS1( 1) H +1(-1)
CPLX 1  1  19.7760  SN+4( 1) HIS1( 1) H +1(-2)
CPLX 0  1  10.7557  SN+4( 1) HIS1( 1) H +1(-3)
CONC
VESL IVOL    25.037  0 0
VESL HIS1   .0007551  2 0
VESL H +1   .0136086  0 0
VESL SN+4   .0006811  0 0
BUR1 H +1  -.0504680  0 0
ELEC
ZERO H +1    405.421    0
GRAD H +1     59.123    0
WGHT 1
VESL HIS1   .0000015
VESL H +1   .0000274
VESL SN+4   .0000014
BUR1 H +1  -.0000100
ZERO H +1       .820
GRAD H +1       .120
TITR RNDE      .0010
EOBS RNDE      .0800
DATA

CONC
```

```
VESL IVOL    24.847  0 0
VESL HIS1   .0013699  2 0
VESL H +1   .0136401  0 0
VESL SN+4   .0006832  0 0
BUR1 H +1  -.0504680  0 0
ELEC
ZERO H +1    402.949    0
GRAD H +1     59.186    0
WGHT 1
VESL HIS1   .0000028
VESL H +1   .0000276
VESL SN+4   .0000014
BUR1 H +1  -.0000100
ZERO H +1       .820
GRAD H +1       .120
TITR RNDE      .0010
EOBS RNDE      .0800
DATA

CONC
VESL IVOL    25.037  0 0
VESL HIS1   .0004422  2 0
VESL H +1   .0135812  0 0
VESL SN+4   .0006795  0 0
BUR1 H +1  -.0504680  0 0
ELEC
ZERO H +1    407.996    0
GRAD H +1     59.172    0
WGHT 1
VESL HIS1   .0000009
VESL H +1   .0000274
VESL SN+4   .0000014
BUR1 H +1  -.0000100
ZERO H +1       .820
GRAD H +1       .120
TITR RNDE      .0010
EOBS RNDE      .0800
DATA


OPTIMIZATION CYCLE  0
**********
OVERALL OBJE OBJECTIVE FUNCTION:    1.1653E+03       (N-R
ITERATIONS:   479)
FORMATION CONSTANTS:
-------------------
```

```
COMPLEX NUMBER:       7         8
 LOG BETA:       27.8638    19.7760

GAUSS-NEWTON:              INITIAL SLOPE =  -1.5261E-04

                    SLOPE AT PREDICTED SOLUTION  =  -3.0857E-06


OPTIMIZATION CYCLE  1
**********
OVERALL OBJE OBJECTIVE FUNCTION:     1.1653E+03       (N-R
ITERATIONS:  1031)
FORMATION CONSTANTS:
-------------------
COMPLEX NUMBER:       7         8
 LOG BETA:       27.8650    19.7771
 STD DEVN:         .2374      .2759

GAUSS-NEWTON:              INITIAL SLOPE =  -7.4167E-07


OPTIMIZATION CYCLE  2    (CONVERGENCE)
**********
OVERALL OBJE OBJECTIVE FUNCTION:     1.1653E+03       (N-R
ITERATIONS:  1585)
FORMATION CONSTANTS:
-------------------
COMPLEX NUMBER:       7         8
 LOG BETA:       27.8650    19.7772
 STD DEVN:         .2375      .2759
NO SIGNIFICANTLY CORRELATED PARAMETERS FOUND
HAMILTON R-FACTOR:   .11329
HAMILTON  R-LIMIT:   .00334
NO. OF TITRATIONS:    3          NO. OF POINTS:  185
Stop - Program terminated.
```

Data for Sn(IV)Cys, more hydrolysis constants included

```
TASK OBJE  1       CYS1-SN+4
MODL     SN+4 CYS1 H +1
CPLX 0  1 -13.7900  SN+4( 0) CYS1( 0) H +1(-1)
CPLX 0  1  10.2803  CYS1( 1) H +1( 1)
CPLX 0  1  18.4262  CYS1( 1) H +1( 2)
CPLX 0  1  19.8815  CYS1( 1) H +1( 3)
CPLX 0  1  -1.9370  SN+4( 1) H +1(-1)
CPLX 0  1  -2.2900  SN+4( 1) H +1(-2)
CPLX 0  1  -3.1700  SN+4( 1) H +1(-3)
CPLX 0  1  -6.3000  SN+4( 1) H +1(-4)
CPLX 0  1 -24.1080  SN+4( 1) H +1(-6)
CPLX 0  1  23.5393  SN+4( 1) CYS1( 1) H +1(-1)
CPLX 1  1  17.6934  SN+4( 1) CYS1( 1) H +1(-2)
CPLX 1  1  10.9523  SN+4( 1) CYS1( 1) H +1(-3)
CONC
VESL IVOL    24.847  0 0
VESL CYS1   .0013786  2 0
VESL H +1   .0150049  0 0
VESL SN+4   .0006956  0 0
BUR1 H +1  -.0504680  0 0
ELEC
ZERO H +1    401.023    0
GRAD H +1     59.154    0
WGHT 1
VESL CYS1   .0000028
VESL H +1   .0000303
VESL SN+4   .0000014
BUR1 H +1  -.0001009
ZERO H +1       .820
GRAD H +1       .120
TITR RNDE      .0010
EOBS RNDE      .0800
DATA

CONC
VESL IVOL    24.848  0 0
VESL CYS1   .0020838  2 0
VESL H +1   .0157023  0 0
VESL SN+4   .0007065  0 0
BUR1 H +1  -.0504680  0 0
ELEC
ZERO H +1    400.444    0
GRAD H +1     59.253    0
WGHT 1
```

```
VESL CYS1   .0000042
VESL H +1   .0000317
VESL SN+4   .0000014
BUR1 H +1  -.0001009
ZERO H +1       .820
GRAD H +1       .120
TITR RNDE      .0010
EOBS RNDE      .0800
DATA

CONC
VESL IVOL     25.037  0 0
VESL CYS1   .0004450  2 0
VESL H +1   .0139770  0 0
VESL SN+4   .0006795  0 0
BUR1 H +1  -.0504680  0 0
ELEC
ZERO H +1    403.079    0
GRAD H +1     59.131    0
WGHT 1
VESL CYS1   .0000009
VESL H +1   .0000282
VESL SN+4   .0000014
BUR1 H +1  -.0000100
ZERO H +1       .820
GRAD H +1       .120
TITR RNDE      .0010
EOBS RNDE      .0800
DATA


OPTIMIZATION CYCLE  0
**********
OVERALL OBJE OBJECTIVE FUNCTION:     1.2624E+03       (N-R
ITERATIONS:   500)
FORMATION CONSTANTS:
--------------------
COMPLEX NUMBER:       11         12
  LOG BETA:        17.6934     10.9523

GAUSS-NEWTON:              INITIAL SLOPE =  -2.0060E-02

                    SLOPE AT PREDICTED SOLUTION  =    6.3442E-03


OPTIMIZATION CYCLE  1
```

```
**********
OVERALL OBJE OBJECTIVE FUNCTION:    1.2613E+03      (N-R
ITERATIONS:  1094)
FORMATION CONSTANTS:
-------------------
COMPLEX NUMBER:      11        12
  LOG BETA:       17.7005   10.9540
  STD DEVN:         .1326     .1328

GAUSS-NEWTON:              INITIAL SLOPE =  -1.9817E-03


OPTIMIZATION CYCLE  2    (CONVERGENCE)
**********
OVERALL OBJE OBJECTIVE FUNCTION:    1.2616E+03      (N-R
ITERATIONS:  1681)
FORMATION CONSTANTS:
-------------------
COMPLEX NUMBER:      11        12
  LOG BETA:       17.6983   10.9535
  STD DEVN:         .1318     .1329
NO SIGNIFICANTLY CORRELATED PARAMETERS FOUND
HAMILTON R-FACTOR:   .11968
HAMILTON  R-LIMIT:   .00339
NO. OF TITRATIONS:    3         NO. OF POINTS:  191
Stop - Program terminated.
```

Sn(IV) His, more hydrolysis constants included

```
TASK OBJE  1       HIS1-SN+4
MODL      SN+4 HIS1 H +1
CPLX 0  1 -13.7900  SN+4( 0) HIS1( 0) H +1(-1)
CPLX 0  1   9.1086  HIS1( 1) H +1( 1)
CPLX 0  1  15.2020  HIS1( 1) H +1( 2)
CPLX 0  1  16.9630  HIS1( 1) H +1( 3)
CPLX 0  1  -1.9370  SN+4( 1) H +1(-1)
CPLX 0  1  -2.2900  SN+4( 1) H +1(-2)
CPLX 0  1  -3.1700  SN+4( 1) H +1(-3)
CPLX 0  1  -6.3000  SN+4( 1) H +1(-4)
CPLX 0  1 -24.1080  SN+4( 1) H +1(-6)
CPLX 0  1  23.5870  SN+4( 1) HIS1( 1) H +1(-1)
CPLX 1  1  17.4764  SN+4( 1) HIS1( 1) H +1(-2)
CPLX 1  1   9.6905  SN+4( 1) HIS1( 1) H +1(-3)
CONC
VESL IVOL     25.037  0 0
VESL HIS1   .0007401  2 0
VESL H +1   .0138098  0 0
VESL SN+4   .0006795  0 0
BUR1 H +1  -.0504680  0 0
ELEC
ZERO H +1    404.983    1
GRAD H +1     58.698    0
WGHT 1
VESL HIS1   .0000015
VESL H +1   .0000274
VESL SN+4   .0000014
BUR1 H +1  -.0000100
ZERO H +1       .820
GRAD H +1       .120
TITR RNDE      .0010
EOBS RNDE      .0800
DATA

CONC
VESL IVOL     24.847  0 0
VESL HIS1   .0013699  2 0
VESL H +1   .0136400  0 0
VESL SN+4   .0006863  0 0
BUR1 H +1  -.0504680  0 0
ELEC
ZERO H +1    399.500    1
GRAD H +1     57.706    0
WGHT 1
```

```
   VESL HIS1   .0000028
   VESL H +1   .0000276
   VESL SN+4   .0000014
   BUR1 H +1  -.0000100
   ZERO H +1       .820
   GRAD H +1       .120
   TITR RNDE      .0010
   EOBS RNDE      .0800
   DATA

   CONC
   VESL IVOL     25.037  0 0
   VESL HIS1   .0004229  2 0
   VESL H +1   .0136149  0 0
   VESL SN+4   .0006795  0 0
   BUR1 H +1  -.0504680  0 0
   ELEC
   ZERO H +1    406.060    1
   GRAD H +1     58.101    0
   WGHT 1
   VESL HIS1   .0000009
   VESL H +1   .0000274
   VESL SN+4   .0000014
   BUR1 H +1  -.0000100
   ZERO H +1       .820
   GRAD H +1       .120
   TITR RNDE      .0010
   EOBS RNDE      .0800
   DATA


OPTIMIZATION CYCLE  0
**********************
OVERALL OBJE OBJECTIVE FUNCTION:    2.6754E+03       (N-R
ITERATIONS:   395)
FORMATION CONSTANTS:
--------------------
COMPLEX NUMBER:       11          12
  LOG BETA:        17.4764      9.6905
LOCAL PARAMETERS:
-----------------
TITRATION   OBJECTIVE       ZERO
 NUMBER     FUNCTION        H +1
    1      1.857E+01     404.983
    2      6.938E+03     399.500
    3      7.181E+02     406.060
```

```
GAUSS-NEWTON:              INITIAL SLOPE =  -2.5703E+03

LEVENBERG-MARQUARDT:       PARAMETER     FRAC.     SLOPE
                    3.995E+02     12.34   -2.5703E+03   0
                    3.995E+02       .73   -1.5347E+02  15

                    SLOPE AT PREDICTED SOLUTION  =   -1.4425E+02


OPTIMIZATION CYCLE  1
*********************
OVERALL OBJE OBJECTIVE FUNCTION:    2.5270E+03       (N-R
ITERATIONS:   791)
FORMATION CONSTANTS:
--------------------
COMPLEX NUMBER:      11         12
 LOG BETA:       17.4638     9.6854
LOCAL PARAMETERS:
-----------------
TITRATION   OBJECTIVE      ZERO
 NUMBER     FUNCTION       H +1
   1      1.667E+01     405.179
   2      6.514E+03     396.586
   3      7.210E+02     406.457

GAUSS-NEWTON:              INITIAL SLOPE =  -2.2730E+03

LEVENBERG-MARQUARDT:       PARAMETER     FRAC.     SLOPE
                    3.966E+02     11.61   -2.2730E+03   0
                    3.966E+02       .73   -1.4436E+02  15

                    SLOPE AT PREDICTED SOLUTION  =   -1.3513E+02


OPTIMIZATION CYCLE  2
*********************
OVERALL OBJE OBJECTIVE FUNCTION:    2.3877E+03       (N-R
ITERATIONS:  1187)
FORMATION CONSTANTS:
--------------------
COMPLEX NUMBER:      11         12
 LOG BETA:       17.4518     9.6800
LOCAL PARAMETERS:
-----------------
TITRATION   OBJECTIVE      ZERO
```

```
 NUMBER    FUNCTION       H +1
   1     1.489E+01    405.375
   2     6.115E+03    393.669
   3     7.239E+02    406.857

GAUSS-NEWTON:              INITIAL SLOPE =  -1.9938E+03

LEVENBERG-MARQUARDT:        PARAMETER     FRAC.     SLOPE
                     3.937E+02     10.88   -1.9938E+03   0
                     3.937E+02      .73   -1.3573E+02  15

                     SLOPE AT PREDICTED SOLUTION  =   -1.2643E+02


OPTIMIZATION CYCLE  3
**********************
OVERALL OBJE OBJECTIVE FUNCTION:    2.2569E+03       (N-R
ITERATIONS:  1584)
FORMATION CONSTANTS:
--------------------
COMPLEX NUMBER:      11         12
 LOG BETA:       17.4405     9.6745
LOCAL PARAMETERS:
-----------------
TITRATION   OBJECTIVE      ZERO
 NUMBER    FUNCTION       H +1
   1     1.321E+01    405.572
   2     5.741E+03    390.739
   3     7.270E+02    407.263

GAUSS-NEWTON:              INITIAL SLOPE =  -1.7319E+03

LEVENBERG-MARQUARDT:        PARAMETER     FRAC.     SLOPE
                     3.907E+02     10.15   -1.7319E+03   0
                     3.907E+02      .74   -1.2752E+02  15

                     SLOPE AT PREDICTED SOLUTION  =   -1.1807E+02


OPTIMIZATION CYCLE  4
**********************
OVERALL OBJE OBJECTIVE FUNCTION:    2.1344E+03       (N-R
ITERATIONS:  1982)
FORMATION CONSTANTS:
--------------------
COMPLEX NUMBER:      11         12
```

```
 LOG BETA:       17.4298     9.6689
LOCAL PARAMETERS:
----------------
TITRATION   OBJECTIVE      ZERO
 NUMBER     FUNCTION       H +1
   1      1.164E+01     405.771
   2      5.391E+03     387.781
   3      7.301E+02     407.675

GAUSS-NEWTON:              INITIAL SLOPE =  -1.4865E+03

LEVENBERG-MARQUARDT:        PARAMETER      FRAC.      SLOPE
                    3.878E+02      9.41   -1.4865E+03   0
                    3.878E+02       .75   -1.1970E+02  15

                    SLOPE AT PREDICTED SOLUTION  =   -1.0999E+02


OPTIMIZATION CYCLE  5
*********************
OVERALL OBJE OBJECTIVE FUNCTION:    2.0198E+03       (N-R
ITERATIONS:  2379)
FORMATION CONSTANTS:
--------------------
COMPLEX NUMBER:      11         12
 LOG BETA:       17.4199     9.6631
LOCAL PARAMETERS:
----------------
TITRATION   OBJECTIVE      ZERO
 NUMBER     FUNCTION       H +1
   1      1.017E+01     405.973
   2      5.063E+03     384.782
   3      7.331E+02     408.096

GAUSS-NEWTON:              INITIAL SLOPE =  -1.2570E+03

LEVENBERG-MARQUARDT:        PARAMETER      FRAC.      SLOPE
                    3.848E+02      8.66   -1.2570E+03   0
                    3.848E+02       .77   -1.1218E+02  15

                    SLOPE AT PREDICTED SOLUTION  =   -1.0210E+02


OPTIMIZATION CYCLE  6
*********************
```

```
OVERALL OBJE OBJECTIVE FUNCTION:    1.9129E+03       (N-R
ITERATIONS:  2777)
FORMATION CONSTANTS:
-------------------
COMPLEX NUMBER:      11         12
 LOG BETA:       17.4107     9.6571
LOCAL PARAMETERS:
----------------
TITRATION   OBJECTIVE      ZERO
 NUMBER     FUNCTION       H +1
   1      8.787E+00     406.180
   2      4.756E+03     381.722
   3      7.360E+02     408.530

GAUSS-NEWTON:              INITIAL SLOPE =  -1.0429E+03

LEVENBERG-MARQUARDT:        PARAMETER      FRAC.      SLOPE
                    3.817E+02      7.90   -1.0429E+03   0
                    3.817E+02       .79   -1.0490E+02  15

                    SLOPE AT PREDICTED SOLUTION  =   -9.4269E+01


OPTIMIZATION CYCLE  7
**********************
OVERALL OBJE OBJECTIVE FUNCTION:    1.8134E+03       (N-R
ITERATIONS:  3175)
FORMATION CONSTANTS:
-------------------
COMPLEX NUMBER:      11         12
 LOG BETA:       17.4025     9.6510
LOCAL PARAMETERS:
----------------
TITRATION   OBJECTIVE      ZERO
 NUMBER     FUNCTION       H +1
   1      7.502E+00     406.392
   2      4.471E+03     378.577
   3      7.387E+02     408.980

GAUSS-NEWTON:              INITIAL SLOPE =  -8.4377E+02

LEVENBERG-MARQUARDT:        PARAMETER      FRAC.      SLOPE
                    3.786E+02      7.11   -8.4377E+02   0
                    3.786E+02       .82   -9.7742E+01  15

                    SLOPE AT PREDICTED SOLUTION  =   -8.6327E+01
```

```
OPTIMIZATION CYCLE  8
*********************
OVERALL OBJE OBJECTIVE FUNCTION:    1.7215E+03      (N-R
ITERATIONS:  3573)
FORMATION CONSTANTS:
--------------------
COMPLEX NUMBER:      11         12
  LOG BETA:       17.3954     9.6448
LOCAL PARAMETERS:
-----------------
TITRATION   OBJECTIVE      ZERO
 NUMBER     FUNCTION       H +1
    1      6.312E+00     406.612
    2      4.208E+03     375.314
    3      7.410E+02     409.451

GAUSS-NEWTON:              INITIAL SLOPE =  -6.5974E+02

LEVENBERG-MARQUARDT:        PARAMETER     FRAC.     SLOPE
                    3.753E+02      6.29   -6.5974E+02   0
                    3.753E+02       .86   -9.0514E+01  15

                    SLOPE AT PREDICTED SOLUTION  =   -7.7988E+01


OPTIMIZATION CYCLE  9
*********************
OVERALL OBJE OBJECTIVE FUNCTION:    1.6372E+03      (N-R
ITERATIONS:  3974)
FORMATION CONSTANTS:
--------------------
COMPLEX NUMBER:      11         12
  LOG BETA:       17.3897     9.6386
LOCAL PARAMETERS:
-----------------
TITRATION   OBJECTIVE      ZERO
 NUMBER     FUNCTION       H +1
    1      5.220E+00     406.843
    2      3.968E+03     371.891
    3      7.426E+02     409.950

GAUSS-NEWTON:              INITIAL SLOPE =  -4.9123E+02

LEVENBERG-MARQUARDT:        PARAMETER     FRAC.     SLOPE
```

```
                    3.719E+02      5.44  -4.9123E+02  0
                    3.719E+02       .91  -8.2891E+01  15

                    SLOPE AT PREDICTED SOLUTION =  -6.8772E+01


OPTIMIZATION CYCLE 10
*********************
OVERALL OBJE OBJECTIVE FUNCTION:    1.5614E+03      (N-R
ITERATIONS:  4376)
FORMATION CONSTANTS:
--------------------
COMPLEX NUMBER:      11        12
  LOG BETA:       17.3861    9.6327
LOCAL PARAMETERS:
-----------------
TITRATION   OBJECTIVE      ZERO
 NUMBER     FUNCTION       H +1
   1      4.235E+00     407.090
   2      3.752E+03     368.252
   3      7.430E+02     410.486

GAUSS-NEWTON:              INITIAL SLOPE =  -3.3953E+02

LEVENBERG-MARQUARDT:       PARAMETER     FRAC.     SLOPE
                    3.683E+02      4.53  -3.3953E+02  0
                    3.683E+02       .98  -7.4226E+01  15

                    SLOPE AT PREDICTED SOLUTION =  -5.7833E+01


OPTIMIZATION CYCLE 11
*********************
OVERALL OBJE OBJECTIVE FUNCTION:    1.4952E+03      (N-R
ITERATIONS:  4779)
FORMATION CONSTANTS:
--------------------
COMPLEX NUMBER:      11        12
  LOG BETA:       17.3858    9.6277
LOCAL PARAMETERS:
-----------------
TITRATION   OBJECTIVE      ZERO
 NUMBER     FUNCTION       H +1
   1      3.376E+00     407.356
   2      3.566E+03     364.322
   3      7.414E+02     411.070
```

```
GAUSS-NEWTON:              INITIAL SLOPE =  -2.0739E+02

LEVENBERG-MARQUARDT:        PARAMETER      FRAC.      SLOPE
                    3.643E+02      3.54   -2.0739E+02   0
                    3.643E+02       .63   -3.7305E+01  16

                    SLOPE AT PREDICTED SOLUTION  =   -3.0505E+01


OPTIMIZATION CYCLE 12
*********************
OVERALL OBJE OBJECTIVE FUNCTION:     1.4612E+03       (N-R
ITERATIONS:  5183)
FORMATION CONSTANTS:
--------------------
COMPLEX NUMBER:       11         12
  LOG BETA:       17.3876     9.6254
LOCAL PARAMETERS:
-----------------
TITRATION   OBJECTIVE      ZERO
 NUMBER     FUNCTION       H +1
    1      2.935E+00     407.527
    2      3.471E+03     361.787
    3      7.392E+02     411.448

GAUSS-NEWTON:              INITIAL SLOPE =  -1.3953E+02

LEVENBERG-MARQUARDT:        PARAMETER      FRAC.      SLOPE
                    3.618E+02      2.91   -1.3953E+02   0
                    3.618E+02       .70   -3.3661E+01  16

                    SLOPE AT PREDICTED SOLUTION  =   -2.5422E+01


OPTIMIZATION CYCLE 13
*********************
OVERALL OBJE OBJECTIVE FUNCTION:     1.4314E+03       (N-R
ITERATIONS:  5586)
FORMATION CONSTANTS:
--------------------
COMPLEX NUMBER:       11         12
  LOG BETA:       17.3926     9.6247
LOCAL PARAMETERS:
-----------------
TITRATION   OBJECTIVE      ZERO
```

```
 NUMBER     FUNCTION       H +1
   1      2.551E+00     407.716
   2      3.391E+03     358.990
   3      7.344E+02     411.863

GAUSS-NEWTON:              INITIAL SLOPE =  -8.0386E+01

LEVENBERG-MARQUARDT:         PARAMETER      FRAC.      SLOPE
                     3.590E+02       2.21   -8.0386E+01   0
                     3.590E+02        .77   -2.8120E+01  16

                     SLOPE AT PREDICTED SOLUTION  =   -1.8131E+01


OPTIMIZATION CYCLE 14
*********************
OVERALL OBJE OBJECTIVE FUNCTION:     1.4080E+03       (N-R
ITERATIONS:  5990)
FORMATION CONSTANTS:
--------------------
COMPLEX NUMBER:       11          12
  LOG BETA:        17.4037      9.6281
LOCAL PARAMETERS:
-----------------
TITRATION   OBJECTIVE       ZERO
 NUMBER     FUNCTION       H +1
   1      2.253E+00     407.924
   2      3.334E+03     355.899
   3      7.245E+02     412.309

GAUSS-NEWTON:              INITIAL SLOPE =  -3.4082E+01

LEVENBERG-MARQUARDT:         PARAMETER      FRAC.      SLOPE
                     3.559E+02       1.44   -3.4082E+01   0
                     3.559E+02        .80   -1.8787E+01  16

                     SLOPE AT PREDICTED SOLUTION  =   -8.2895E+00


OPTIMIZATION CYCLE 15
*********************
OVERALL OBJE OBJECTIVE FUNCTION:     1.3941E+03       (N-R
ITERATIONS:  6397)
FORMATION CONSTANTS:
--------------------
COMPLEX NUMBER:       11          12
```

```
 LOG BETA:       17.4267     9.6429
LOCAL PARAMETERS:
----------------
TITRATION   OBJECTIVE      ZERO
 NUMBER     FUNCTION       H +1
   1      2.083E+00     408.136
   2      3.314E+03     352.713
   3      7.039E+02     412.714

GAUSS-NEWTON:              INITIAL SLOPE =  -6.9844E+00

                       SLOPE AT PREDICTED SOLUTION  =   -2.4892E-02


OPTIMIZATION CYCLE 16
*********************
OVERALL OBJE OBJECTIVE FUNCTION:     1.3904E+03       (N-R
ITERATIONS:  6803)
FORMATION CONSTANTS:
--------------------
COMPLEX NUMBER:      11         12
 LOG BETA:       17.4743     9.6915
LOCAL PARAMETERS:
----------------
TITRATION   OBJECTIVE      ZERO
 NUMBER     FUNCTION       H +1
   1      2.042E+00     408.296
   2      3.347E+03     350.153
   3      6.574E+02     412.764

GAUSS-NEWTON:              INITIAL SLOPE =  -3.8138E-03

                       SLOPE AT PREDICTED SOLUTION  =   -9.8359E-06


OPTIMIZATION CYCLE 17
*********************
OVERALL OBJE OBJECTIVE FUNCTION:     1.3903E+03       (N-R
ITERATIONS:  7277)
FORMATION CONSTANTS:
--------------------
COMPLEX NUMBER:      11         12
 LOG BETA:       17.4765     9.6906
 STD DEVN:         .1610       .2222
LOCAL PARAMETERS:
----------------
```

```
TITRATION   OBJECTIVE      ZERO
 NUMBER     FUNCTION       H +1
   1      2.042E+00     408.296
   2      3.347E+03     350.150
   3      6.565E+02     412.755
STANDARD DEVIATIONS:
--------------------
TITRATION                ZERO
 NUMBER                  H +1
   1                   3.203
   2                   3.216
   3                   3.540

GAUSS-NEWTON:              INITIAL SLOPE =  -1.5130E-05


OPTIMIZATION CYCLE 18    (CONVERGENCE)
**********************
OVERALL OBJE OBJECTIVE FUNCTION:     1.3903E+03       (N-R
ITERATIONS:  7755)
FORMATION CONSTANTS:
--------------------
COMPLEX NUMBER:       11          12
  LOG BETA:        17.4764      9.6905
  STD DEVN:         .1610       .2223
LOCAL PARAMETERS:
-----------------
TITRATION   OBJECTIVE      ZERO
 NUMBER     FUNCTION       H +1
   1      2.042E+00     408.296
   2      3.347E+03     350.151
   3      6.566E+02     412.752
STANDARD DEVIATIONS:
--------------------
TITRATION                ZERO
 NUMBER                  H +1
   1                   3.203
   2                   3.216
   3                   3.540
NO SIGNIFICANTLY CORRELATED PARAMETERS FOUND
HAMILTON R-FACTOR:   .12902
HAMILTON  R-LIMIT:   .00352
NO. OF TITRATIONS:    3         NO. OF POINTS:  139
Stop - Program terminated.
```